CHAPTER 5

Filter Bank Methods

5.1 INTRODUCTION

The problem of estimating the PSD function $\phi(\omega)$ of a signal from a finite number of observations N is ill posed from a statistical standpoint, *unless* we make some appropriate assumptions on $\phi(\omega)$. More precisely, without any assumption on the PSD we are required to estimate an *infinite* number of independent values $\{\phi(\omega)\}_{\omega=-\pi}^{\pi}$ from a *finite* number of samples. Evidently, we cannot do that in a consistent manner. In order to overcome this problem, we can either

Parameterize $\{\phi(\omega)\}$ by means of a finite–dimensional model	(5.1.1)

or

Smooth the set $\{\phi(\omega)\}_{\omega=-\pi}^{\pi}$ by assuming that $\phi(\omega)$ is constant (or nearly constant) over the band $[\omega - \beta\pi, \omega + \beta\pi]$, for some given $\beta \ll 1$.	(5.1.2)

The approach based on (5.1.1) leads to the parametric spectral methods of Chapters 3 and 4, for which the estimation of $\{\phi(\omega)\}$ is reduced to the problem of estimating a number of parameters that is usually much smaller than the data length N.

The other approach to PSD estimation, (5.1.2), leads to the methods to be described in this chapter. The nonparametric methods of Chapter 2 are also (implicitly) based on (5.1.2), as shown in Section 5.2. The approach (5.1.2) should, of course, be used for PSD estimation when we do not have enough information about the studied signal to be able to describe it (and its PSD) by a simple model (such as the ARMA equation in Chapter 3 or the equation of superimposed sinusoidal signals in Chapter 4). On one hand, this implies that the methods derived from (5.1.2) can be used in cases where those based on (5.1.1) cannot.[1] On the other hand, we should expect to pay some price in using (5.1.2) over (5.1.1). Under the assumption in (5.1.2), $\phi(\omega)$ is described by $2\pi/2\pi\beta = 1/\beta$ values. In order to estimate these values from the available data in a consistent manner, we must require

[1] This statement should be interpreted with some care. One can certainly use, for instance, an ARMA spectral model even if one does not know that the studied signal is really an ARMA signal. However, in such a case one does not only have to estimate the model parameters but must also face the rather difficult task of determining the structure of the parametric model used (for example, the orders of the ARMA model). The nonparametric approach to PSD estimation does not require any structure determination step.

that $1/\beta < N$ or

$$N\beta > 1 \tag{5.1.3}$$

As β increases, the achievable statistical accuracy of the estimates of $\{\phi(\omega)\}$ should increase (because the number of PSD values estimated from the given N data samples decreases) but the resolution decreases (because $\phi(\omega)$ is assumed to be constant on a larger interval). This *tradeoff between statistical variability and resolution* is the price paid for the generality of the methods derived from (5.1.2). We already met this tradeoff in our discussion of the periodogram–based methods in Chapter 2. Note from (5.1.3) that the *resolution threshold* β of the methods based on (5.1.2) can be lowered down to $1/N$ only if we are going to accept a significant statistical variability for our spectral estimates (because for $\beta = 1/N$ we will have to estimate N spectral values from the available N data samples). The parametric (or model–based) approach embodied in (5.1.1) describes the PSD by a number of parameters that is often much smaller than N, and yet it may achieve better resolution (*i.e.*, a resolution threshold less than $1/N$) compared to the approach derived from (5.1.2).

When taking the approach (5.1.2) to PSD estimation, we are basically following the "definition" (1.1.1) of the spectral estimation problem, which we restate here (in abbreviated form) for easy reference:

From a finite–length data sequence, estimate how the power is distributed over narrow spectral bands. (5.1.4)

There is an implicit assumption in (5.1.4) that the power is (nearly) constant over "narrow spectral bands", which is a restatement of (5.1.2).

The most natural implementation of the approach to spectral estimation resulting from (5.1.2) and (5.1.4) is depicted in Figure 5.1. The bandpass filter in this figure, which sweeps through the frequency interval of interest, can be viewed as a bank of (bandpass) filters. This observation motivates the name of *filter bank approach* given to the PSD estimation scheme sketched in Figure 5.1. Depending on the bandpass filter chosen, we may obtain various filter bank methods of spectral estimation. Even for a given bandpass filter, we may implement the scheme of Figure 5.1 in different ways, which leads to an even richer class of methods. Examples of bandpass filters that can be used in the scheme of Figure 5.1, as well as specific ways in which they may be implemented, are given in the remainder of this chapter. First, however, we discuss a few more aspects regarding the scheme in Figure 5.1.

As a mathematical motivation of the filter bank approach (FBA) to spectral

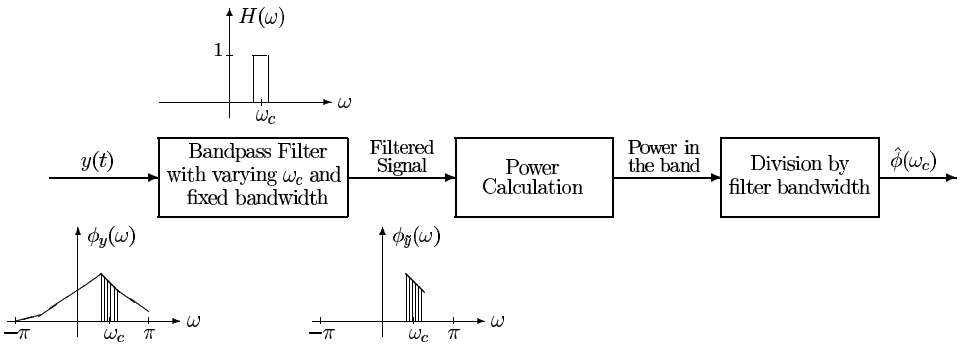

Figure 5.1. The filter bank approach to PSD estimation.

estimation, we prove the following result.

Assume that:

(i) $\phi(\omega)$ is (nearly) constant over the filter passband;

(ii) The filter gain is (nearly) one over the passband and (nearly) zero outside the passband; *and*

(iii) The power of the filtered signal is consistently estimated.

Then:

The PSD estimate, $\hat{\phi}_{\mathrm{FB}}(\omega)$, obtained with the filter bank approach, is a good approximation of $\phi(\omega)$.

(5.1.5)

Let $H(\omega)$ denote the transfer function of the bandpass filter, and let $2\pi\beta$ denote its bandwidth. Then by using the formula (1.4.9) and the assumptions (iii), (ii) and (i) (in that order), we can write

$$\begin{aligned}\hat{\phi}_{\mathrm{FB}}(\omega) &\simeq \frac{1}{2\pi\beta}\int_{-\pi}^{\pi} |H(\psi)|^2\phi(\psi)\,d\psi \\ &\simeq \frac{1}{2\pi\beta}\int_{\omega-\beta\pi}^{\omega+\beta\pi} \phi(\psi)\,d\psi \simeq \frac{1}{2\pi\beta}2\pi\beta\phi(\omega) = \phi(\omega)\end{aligned} \tag{5.1.6}$$

where ω denotes the center frequency of the bandpass filter. This is the result which we set out to prove.

If all three assumptions in (5.1.5) could be satisfied, then the FBA methods would produce spectral estimates with high resolution and low statistical variability. Unfortunately, these assumptions contain conflicting requirements that cannot be met simultaneously. In high–resolution applications, assumption (i) can be satisfied

if we use a filter with a *very sharp passband*. According to the time–bandwidth product result (2.6.5), such a filter has a very long impulse response. This implies that we may be able to get only a few samples of the filtered signal (sometimes only one sample, see Section 5.2!). Hence, assumption (iii) cannot be met. In order to satisfy (iii), we need to average many samples of the filtered signal and, therefore, should consider a bandpass filter with a relatively short impulse response and hence a not too narrow passband. Assumption (i) may then be violated or, in other words, the resolution may be sacrificed.

The above discussion has brought once more to light *the compromise between resolution and statistical variability* and the fact that *the resolution is limited by the sample length*. These are the critical issues for any PSD estimation method based on the approach (5.1.2), such as those of Chapter 2 and the ones discussed in the following sections. The previous two issues will always surface within the nonparametric approach to spectral estimation, in many different ways depending on the specific method at hand.

5.2 FILTER BANK INTERPRETATION OF THE PERIODOGRAM

The value of the basic periodogram estimator (2.2.1) at a given frequency, say $\tilde{\omega}$, can be expressed as

$$\begin{aligned}\hat{\phi}_p(\tilde{\omega}) &= \frac{1}{N}\left|\sum_{t=1}^{N} y(t)e^{-i\tilde{\omega}t}\right|^2 = \frac{1}{N}\left|\sum_{t=1}^{N} y(t)e^{i\tilde{\omega}(N-t)}\right|^2 \\ &= \frac{1}{\beta}\left|\sum_{k=0}^{N-1} h_k y(N-k)\right|^2 \end{aligned} \tag{5.2.1}$$

where $\beta = 1/N$ and

$$h_k = \frac{1}{N}e^{i\tilde{\omega}k} \qquad k = 0, \ldots, N-1 \tag{5.2.2}$$

The *truncated* convolution sum that appears in (5.2.1) can be written as the usual convolution sum associated with a linear causal system, if the weighting sequence in (5.2.2) is padded with zeroes:

$$y_F(N) = \sum_{k=0}^{\infty} h_k y(N-k) \tag{5.2.3}$$

with

$$h_k = \begin{cases} e^{i\tilde{\omega}k}/N & \text{for } \; k = 0, \ldots, N-1 \\ 0 & \text{otherwise} \end{cases} \tag{5.2.4}$$

The transfer function (or the frequency response) of the linear filter corresponding to $\{h_k\}$ in (5.2.4) is readily evaluated:

$$H(\omega) = \sum_{k=0}^{\infty} h_k e^{-i\omega k} = \frac{1}{N}\sum_{k=0}^{N-1} e^{i(\tilde{\omega}-\omega)k} = \frac{1}{N}\,\frac{e^{iN(\tilde{\omega}-\omega)}-1}{e^{i(\tilde{\omega}-\omega)}-1}$$

which gives

$$H(\omega) = \frac{1}{N} \frac{\sin[N(\tilde{\omega} - \omega)/2]}{\sin[(\tilde{\omega} - \omega)/2]} e^{i(N-1)(\tilde{\omega}-\omega)/2} \tag{5.2.5}$$

Figure 5.2 shows $|H(\omega)|$ as a function of $\Delta\omega = \tilde{\omega} - \omega$, for $N = 50$. It can be seen that $H(\omega)$ in (5.2.5) is the transfer function of a bandpass filter with center frequency equal to $\tilde{\omega}$. The *3dB bandwidth* of this filter can be shown to be approximately $2\pi/N$ radians per sampling interval, or $1/N$ cycles per sampling interval. In fact, by comparing (5.2.5) to (2.4.17) we see that $H(\omega)$ resembles the DTFT of the rectangular window, the only differences being the phase term (due to the time offset) and the window lengths ($(2N-1)$ in (2.4.17) versus N in (5.2.5)).

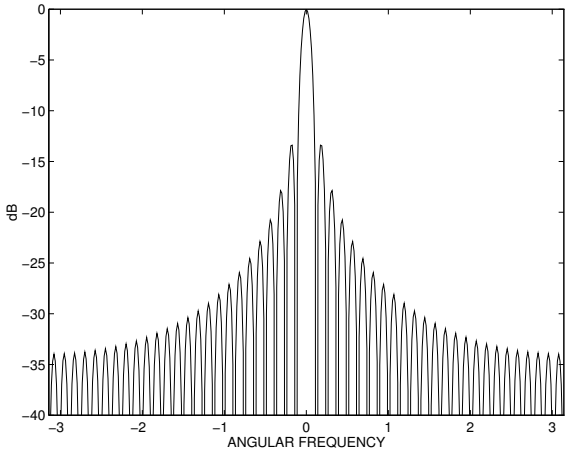

Figure 5.2. The magnitude of the frequency response of the bandpass filter $H(\omega)$ in (5.2.5), associated with the periodogram ($N = 50$), plotted as a function of $(\tilde{\omega} - \omega)$.

Thus, we have proven the following *filter bank interpretation of the basic periodogram.*

> The periodogram $\hat{\phi}_p(\omega)$ can be exactly obtained by the FBA in Figure 5.1, where the bandpass filter's frequency response is given by (5.2.5), its bandwidth is $1/N$ cycles per sampling interval, and the power calculation is done from a *single sample* of the filtered signal. (5.2.6)

This interpretation of $\hat{\phi}_p(\omega)$ highlights a conclusion that is reached, in a different way, in Chapter 2: *the unmodified periodogram sacrifices statistical accuracy for resolution.* Indeed, $\hat{\phi}_p(\omega)$ uses a bandpass filter with the smallest bandwidth afforded by a time aperture of length N. In this way, it achieves a good resolution

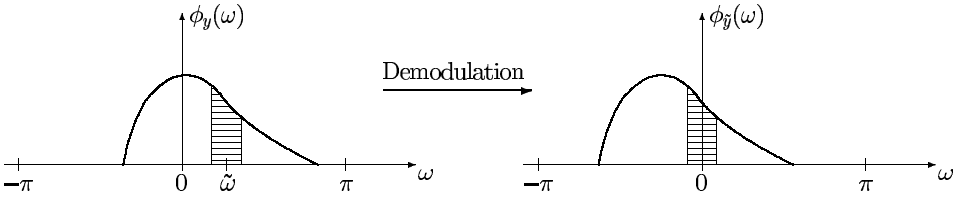

Figure 5.3. The relationship between the PSDs of the original signal $y(t)$ and the demodulated signal $\tilde{y}(t)$.

(see assumption (i) in (5.1.5)). The consequence of doing so is that only one (filtered) data sample is obtained for the power calculation stage, which explains the erratic fluctuations of $\hat{\phi}_p(\omega)$ (owing to violation of assumption (iii) in (5.1.5)).

As explained in Chapter 2, the *modified periodogram methods* (Bartlett, Welch and Daniell) reduce the variance of the periodogram at the expense of increasing the bias (or, equivalently, worsening the resolution). The FBA interpretation of these modified methods provides an interesting explanation of their behavior. In the filter bank context, the basic idea behind all of these modified periodograms is *to improve the power calculation stage* which is done so poorly within the unmodified periodogram.

The Bartlett and Welch methods split the available sample in several stretches which are separately (bandpass) filtered. In principle, the larger the number of stretches, the more samples are averaged in the power calculation stage and the smaller the variance of the estimated PSD, but the worse the resolution (owing to the inability to design an appropriately narrow bandpass filter for a small–aperture stretch).

The Daniell method, on the other hand, does not split the sample of observations but processes it as a whole. This method improves the "power calculation" in a different way. For each value of $\phi(\omega)$ to be estimated, a number of different bandpass filters are employed, each with center frequency near ω. Each bandpass filter yields only one sample of the filtered signal, but as there are several bandpass filters we may get enough information for the power calculation stage. As the number of filters used increases, the variance of the estimated PSD decreases but the resolution becomes worse (since $\phi(\omega)$ is implicitly assumed to be constant over a wider and wider frequency interval centered on the current ω and approximately equal to the union of the filters' passbands).

5.3 REFINED FILTER BANK METHOD

The bandpass filter used in the periodogram is nothing but one of many possible choices. Since the periodogram was *not* designed as a filter bank method, we may wonder whether we could not find other better choices of the bandpass filter. In this section, we present a refined filter bank (RFB) approach to spectral estimation. Such an approach was introduced in [Thomson 1982] and was further developed in [Mullis and Scharf 1991] (more recent references on this approach include [Bronez 1992; Onn and Steinhardt 1993; Riedel and Sidorenko 1995]).

For the discussion that follows, it is convenient to use a *baseband filter* in the

filter bank approach of Figure 5.1, in lieu of the bandpass filter. Let $H_{\mathrm{BF}}(\omega)$ denote the frequency response of the bandpass filter with center frequency $\tilde{\omega}$ (say), and let the baseband filter be defined by:

$$H(\omega) = H_{\mathrm{BF}}(\omega + \tilde{\omega}) \tag{5.3.1}$$

(the center frequency of $H(\omega)$ is equal to zero). If the input to the FBA scheme is also modified in the following way,

$$\boxed{y(t) \longrightarrow \tilde{y}(t) = e^{-i\tilde{\omega}t} y(t)} \tag{5.3.2}$$

then, according to the complex (de)modulation formula (1.4.11), the output of the scheme is left unchanged by the translation in (5.3.1) of the passband down to baseband. In order to help interpret the transformations above, we depict in Figure 5.3 the type of PSD translation implied by the *demodulation process* in (5.3.2). It is clearly seen from this figure that the problem of isolating the band around $\tilde{\omega}$ by bandpass filtering becomes one of baseband filtering. The modified FBA scheme is shown in Figure 5.4. The baseband filter design problem is the subject of the next subsection.

5.3.1 Slepian Baseband Filters

In the following, we address the problem of designing a finite impulse response (FIR) baseband filter which passes the *baseband*

$$[-\beta\pi, \beta\pi] \tag{5.3.3}$$

as undistorted as possible, and which attenuates the frequencies outside baseband as much as possible. Let

$$h = [h_0 \dots h_{N-1}]^* \tag{5.3.4}$$

denote the impulse response of such a filter, and let

$$H(\omega) = \sum_{k=0}^{N-1} h_k e^{-i\omega k} = h^* a(\omega)$$

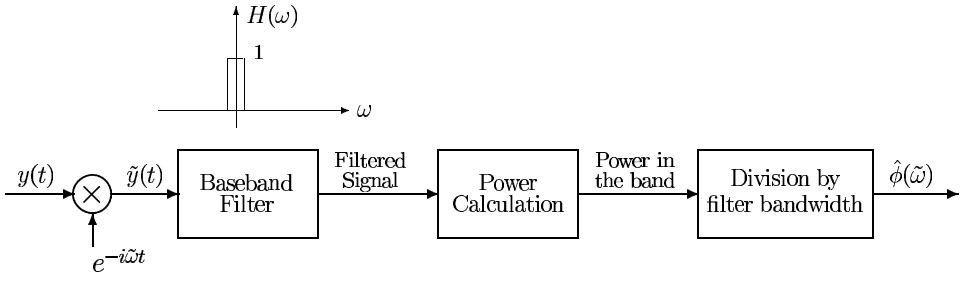

Figure 5.4. The modified filter bank approach to PSD estimation.

(where $a(\omega) = [1 \; e^{-i\omega} \ldots \; e^{-i(N-1)\omega}]^T$) be the corresponding frequency response. The two design objectives can be turned into mathematical specifications in the following way. Let the input to the filter be *white noise* of unit variance. Then the power of the output is:

$$\begin{aligned}\frac{1}{2\pi}\int_{-\pi}^{\pi}|H(\omega)|^2 d\omega &= \sum_{k=0}^{N-1}\sum_{p=0}^{N-1} h_k h_p^* \left[\frac{1}{2\pi}\int_{-\pi}^{\pi} e^{i\omega(p-k)}d\omega\right] \\ &= \sum_{k=0}^{N-1}\sum_{p=0}^{N-1} h_k h_p^* \delta_{k,p} = h^* h \end{aligned} \tag{5.3.5}$$

We note in passing that equation (5.3.5) above can be recognized as the Parseval's theorem (1.2.6). The part of the total power, (5.3.5), that lies in the baseband is given by

$$\frac{1}{2\pi}\int_{-\beta\pi}^{\beta\pi}|H(\omega)|^2 d\omega = h^*\left\{\frac{1}{2\pi}\int_{-\beta\pi}^{\beta\pi} a(\omega)a^*(\omega)d\omega\right\} h \triangleq h^*\Gamma h \tag{5.3.6}$$

The k,p element of the $N \times N$ matrix Γ defined in (5.3.6) is given by

$$\Gamma_{k,p} = \frac{1}{2\pi}\int_{-\beta\pi}^{\beta\pi} e^{-i(k-p)\omega}d\omega = \frac{\sin[(k-p)\beta\pi]}{(k-p)\pi} \tag{5.3.7}$$

which, using the sinc function, can be written as

$$\boxed{\Gamma_{k,p} = \beta\text{sinc}[(k-p)\beta\pi] \triangleq \gamma_{|k-p|}} \tag{5.3.8}$$

Note that the matrix Γ is symmetric and Toeplitz. Also, note that this matrix has already been encountered in the window design example in Section 2.6.3. In fact, as we will shortly see, the window design strategy in that example is quite similar to the baseband filter design method employed here.

Since the filter h must be such that the power of the filtered signal in the baseband is as large as possible relative to the total power, we are led to the following optimization problem:

$$\boxed{\max_h h^*\Gamma h \qquad \text{subject to} \quad h^*h = 1} \tag{5.3.9}$$

The solution to the problem above is given in Result R13 in Appendix A: the maximizing h is equal to the eigenvector of Γ corresponding to its maximum eigenvalue. Hence, we have proven the following result.

The impulse response h of the "most selective" baseband filter (according to the design objectives in (5.3.9)) is given by the dominant eigenvector of Γ, and is called the *first Slepian sequence.* (5.3.10)

The matrix Γ played a key role in the foregoing derivation. In what follows, we look in more detail at the *eigenstructure of* Γ. In particular, we provide an intuitive explanation as to why the first dominant eigenvector of Γ behaves like a baseband filter. We also show that, depending on the relation between β and N, the next dominant eigenvectors of Γ might also be used as baseband filters. Our discussion of these aspects will be partly heuristic. Note that the eigenvectors of Γ are called the *Slepian sequences* [SLEPIAN 1964] (as already indicated in (5.3.10)). We denote these eigenvectors by $\{s_k\}_{k=1}^{N}$.

Remark: The Slepian sequences should not be computed by the eigendecomposition of Γ. Numerically more efficient and reliable ways for computing these sequences exist (see, *e.g.*, [SLEPIAN 1964]), for instance as solutions to some differential equations or as eigenvectors of certain tridiagonal matrices. ■

The theoretical eigenanalysis of Γ is a difficult problem in the case of finite N. (Of course, the eigenvectors and eigenvalues of Γ may always be *computed*, for given β and N; here we are interested in establishing *theoretical expressions* for Γ's eigenelements.) For N sufficiently large, however, "reasonable approximations" to the eigenelements of Γ can be derived. Let $a(\omega)$ be defined as before:

$$a(\omega) = [1 \;\; e^{-i\omega} \ldots \; e^{-i(N-1)\omega}]^T \tag{5.3.11}$$

Assume that β is *chosen larger than* $1/N$, and define

$$\boxed{K = N\beta \geq 1} \tag{5.3.12}$$

(To simplify the discussion, K and N are assumed to be even integers in what follows.) With these preparations and assuming that N is large, we can approximate the integral in (5.3.6) and write Γ as

$$\begin{aligned}\Gamma &\simeq \frac{1}{2\pi} \sum_{p=-K/2}^{K/2-1} a\left(\frac{2\pi}{N}p\right) a^*\left(\frac{2\pi}{N}p\right) \frac{2\pi}{N} \\ &= \frac{1}{N} \sum_{p=-K/2}^{K/2-1} a\left(\frac{2\pi}{N}p\right) a^*\left(\frac{2\pi}{N}p\right) \triangleq \Gamma_0\end{aligned} \tag{5.3.13}$$

The vectors $\{a(\frac{2\pi}{N}p)/\sqrt{N}\}_{p=-\frac{N}{2}+1}^{\frac{N}{2}}$, part of which appears in (5.3.13), can be readily shown to form an *orthonormal set*:

$$\begin{aligned}\frac{1}{N} a^*\left(\frac{2\pi}{N}p\right) a\left(\frac{2\pi}{N}s\right) &= \frac{1}{N} \sum_{k=0}^{N-1} e^{i\frac{2\pi}{N}(p-s)k} \\ &= \begin{cases} \dfrac{1}{N} \dfrac{e^{i2\pi(p-s)} - 1}{e^{i\frac{2\pi}{N}(p-s)} - 1} = 0, & s \neq p \\ 1, & s = p \end{cases}\end{aligned} \tag{5.3.14}$$

The eigenvectors of the matrix on the right hand side of equation (5.3.13), Γ_0, are therefore given by $\{a\left(\frac{2\pi}{N}p\right)/\sqrt{N}\}_{p=-N/2+1}^{N/2}$, with eigenvalues of 1 (with multiplicity K) and 0 (with multiplicity $N-K$). The eigenvectors corresponding to the eigenvalues equal to one are $\{a\left(\frac{2\pi}{N}p\right)/\sqrt{N}\}_{p=-K/2+1}^{K/2}$. By paralleling the calculations in (5.2.3)–(5.2.5), it is not hard to show that each of these dominant eigenvectors of Γ_0 is the impulse response of a narrow bandpass filter with bandwidth equal to about $1/N$ and center frequency $\frac{2\pi}{N}p$; the set of these filters therefore covers the interval $[-\beta\pi, \beta\pi]$.

Now, the elements of Γ approach those of Γ_0 as N increases; more precisely, $|[\Gamma]_{i,j} - [\Gamma_0]_{i,j}| = \mathcal{O}(1/N)$ for sufficiently large N. However, this does *not* mean that $\|\Gamma - \Gamma_0\| \to 0$, as $N \to \infty$, for any reasonable matrix norm, because Γ and Γ_0 are $(N \times N)$ matrices. Consequently, the eigenelements of Γ do *not* necessarily converge to the eigenelements of Γ_0 as $N \to \infty$. However, based on the previous analysis, we can at least expect that the eigenelements of Γ are not "too different" from those of Γ_0. This observation of the theoretical analysis, backed up with empirical evidence from the computation of the eigenelements of Γ in specific cases, leads us to conclude the following.

> The matrix Γ has K eigenvalues close to one and $(N-K)$ eigenvalues close to zero, provided N is large enough, where K is given by the "time–bandwidth" product (5.3.12). The dominant eigenvectors corresponding to the K largest eigenvalues form a set of orthogonal impulse responses of K bandpass filters that approximately cover the baseband $[-\beta\pi, \beta\pi]$. (5.3.15)

As we argue in the next subsections, in some situations (specified there) we may want to use the whole set of K *Slepian baseband filters*, not only the dominant Slepian filter in this set.

5.3.2 RFB Method for High–Resolution Spectral Analysis

Assume that the spectral analysis problem dealt with is one in which it is important to achieve the maximum resolution afforded by the approach at hand (such a problem appears, for instance, in the case of PSD's with closely spaced peaks). Then we set

$$\beta = 1/N \Longleftrightarrow K = 1 \tag{5.3.16}$$

(Note that we cannot set β to a value less than $1/N$ since that choice would lead to $K < 1$, which is meaningless; the fact that we must choose $\beta \geq 1/N$ is one of the many facets of the $1/N$–resolution limit of the nonparametric spectral estimation.)

Since $K = 1$, we can only use the first Slepian sequence as a bandpass filter

$$h = s_1 \tag{5.3.17}$$

The way in which the RFB scheme based on (5.3.17) works is described in the following.

First, note from (5.3.5), (5.3.9) and (5.3.16) that

$$1 = h^*h = \frac{1}{2\pi}\int_{-\pi}^{\pi}|H(\omega)|^2 d\omega \simeq \frac{1}{2\pi}\int_{-\beta\pi}^{\beta\pi}|H(\omega)|^2 d\omega$$
$$\simeq \beta|H(0)|^2 = \frac{1}{N}|H(0)|^2 \tag{5.3.18}$$

Hence, under the (idealizing) assumption that $H(\omega)$ is different from zero only in the baseband where it takes a constant value, we have

$$|H(0)|^2 \simeq N \tag{5.3.19}$$

Next, consider the sample at the filter's output obtained by the convolution of the whole input sequence $\{\tilde{y}(t)\}_{t=1}^{N}$ with the filter impulse response $\{h_k\}$:

$$x \triangleq \sum_{k=0}^{N-1} h_k \tilde{y}(N-k) = \sum_{t=1}^{N} h_{N-t}\tilde{y}(t) \tag{5.3.20}$$

The power of x should be approximately equal to the PSD value $\phi(\tilde{\omega})$, which is confirmed by the following calculation:

$$E\left\{|x|^2\right\} = \frac{1}{2\pi}\int_{-\pi}^{\pi}|H(\omega)|^2\phi_{\tilde{y}}(\omega)d\omega$$
$$\simeq \frac{N}{2\pi}\int_{-\beta\pi}^{\beta\pi}\phi_{\tilde{y}}(\omega)d\omega = \frac{N}{2\pi}\int_{-\beta\pi}^{\beta\pi}\phi_y(\omega+\tilde{\omega})d\omega$$
$$\simeq \frac{N}{2\pi}\phi_y(\tilde{\omega}) \times 2\pi\beta = N\beta\phi_y(\tilde{\omega}) = \phi_y(\tilde{\omega}) \tag{5.3.21}$$

The second "equality" above follows from the properties of $H(\omega)$ (see, also, (5.3.19)), the third from the complex demodulation formula (1.4.11), and the fourth from the assumption that $\phi_y(\omega)$ is nearly constant over the passband considered.

In view of (5.3.21), the PSD estimation problem reduces to estimating the power of the filtered signal. Since only one sample, x, of that signal is available, the obvious estimate for the signal power is $|x|^2$. This leads to the following estimate of $\phi(\omega)$:

$$\boxed{\hat{\phi}(\omega) = \left|\sum_{t=1}^{N} h_{N-t}y(t)e^{-i\omega t}\right|^2} \tag{5.3.22}$$

where $\{h_k\}$ is given by the first Slepian sequence (see (5.3.17)). The reason we did not divide (5.3.22) by the filter bandwidth is that $|H(0)|^2 \simeq N$ by (5.3.19), which differs from assumption (ii) in (5.1.5).

The spectral estimate (5.3.22) is recognized to be a *windowed periodogram* with *temporal window* $\{h_{N-k}\}$. For large values of N, it follows from the analysis in the previous section that h can be expected to be reasonably close to the vector $[1\ldots1]^T/\sqrt{N}$. When inserting the latter vector in (5.3.22), we get the unwindowed

periodogram. Hence, we reach the conclusion that *for N large enough, the RFB estimate* (5.3.22) *will behave not too differently from the unmodified periodogram* (which is quite natural in view of the fact that we wanted a high–resolution spectral estimator, and the basic periodogram is known to be such an estimator).

Remark: We warn the reader, once again, that the above discussion is heuristic. As explained before (see the discussion related to (5.3.15)), as N increases $\{h_k\}$ may be expected to be "reasonably close" but not necessarily converge to $1/\sqrt{N}$. In addition, even if $\{h_k\}$ in (5.3.22) converges to $1/\sqrt{N}$ as $N \to \infty$, the function in (5.3.22) may not converge to $\hat{\phi}_p(\omega)$ if the convergence *rate* of $\{h_k\}$ is too slow (note that the number of $\{h_k\}$ in (5.3.22) is equal to N). Hence $\hat{\phi}(\omega)$ in (5.3.22) and the periodogram $\hat{\phi}_p(\omega)$ may differ from one another even for large values of N. ■

In any case, even though the two estimators $\hat{\phi}(\omega)$ in (5.3.22) and $\hat{\phi}_p(\omega)$ generally give different PSD values, they both base the power calculation stage of the FBA scheme on only a single sample. Hence, similarly to $\hat{\phi}_p(\omega)$, the RFB estimate (5.3.22) is expected to exhibit erratic fluctuations. The next subsection discusses a way in which the variance of the RFB spectral estimate can be reduced, at the expense of reducing the resolution of this estimate.

5.3.3 RFB Method for Statistically Stable Spectral Analysis

The FBA interpretation of the modified periodogram methods, as explained in Section 5.2, highlighted two approaches to reduce the statistical variability of the spectral estimate (5.3.22). The *first approach* consists of splitting the available sample $\{y(t)\}_{t=1}^{N}$ into a number of subsequences, computing (5.3.22) for each stretch, and then averaging the so–obtained values. The problem with this way of proceeding is that the values taken by (5.3.22) for different subsequences are not guaranteed to be statistically independent. In fact, if the subsequences overlap then those values may be strongly correlated. The consequence of this fact is that one can never be sure of the "exact" reduction of variance that is achieved by averaging, in a given situation.

The *second approach* to reduce the variance consists of using several bandpass filters, in lieu of only one, which operate on the whole data sample [THOMSON 1982]. This approach aims at producing *statistically independent samples for the power calculation stage*. When this is achieved *the variance is reduced K times*, where K is the number of samples averaged (which equals the number of bandpass filters used).

In the following, we focus on this second approach which appears particularly suitable for the RFB method. We set β to some value larger than $1/N$, which gives (*cf.* (5.3.12))

$$\boxed{K = N\beta > 1} \tag{5.3.23}$$

The larger β (*i.e.*, the lower the resolution), the larger K and hence the larger the reduction in variance that can be achieved. By using the result (5.3.15), we define

K baseband filters as

$$\boxed{h_p = [h_{p,0} \dots h_{p,N-1}]^* = s_p, \qquad (p = 1, \dots, K)} \tag{5.3.24}$$

Here h_p denotes the impulse response vector of the pth filter, and s_p is the pth dominant Slepian sequence. Note that s_p is real–valued (see Result R12 in Appendix A), and thus so is h_p. According to the discussion leading to (5.3.15), the set of filters (5.3.24) covers the baseband $[-\beta\pi, \beta\pi]$, with each of these filters passing (roughly speaking) $(1/K)$th of this baseband. Let x_p be defined similarly to x in (5.3.20), but now for the pth filter:

$$x_p = \sum_{k=0}^{N-1} h_{p,k}\tilde{y}(N-k) = \sum_{t=1}^{N} h_{p,N-t}\tilde{y}(t) \tag{5.3.25}$$

The calculation (5.3.21) applies to $\{x_p\}$ in exactly the same way, and hence

$$E\left\{|x_p|^2\right\} \simeq \phi_y(\tilde{\omega}), \qquad p = 1, \dots, K \tag{5.3.26}$$

In addition, a straightforward calculation gives

$$\begin{aligned}
E\{x_p x_k^*\} &= E\left\{\left[\sum_{t=0}^{N-1} h_{p,t}\tilde{y}(N-t)\right]\left[\sum_{s=0}^{N-1} h_{k,s}^*\tilde{y}^*(N-s)\right]\right\} \\
&= \sum_{t=0}^{N-1}\sum_{s=0}^{N-1} h_{p,t}h_{k,s}^* r_{\tilde{y}}(s-t) \\
&= \frac{1}{2\pi}\int_{-\pi}^{\pi}\sum_{t=0}^{N-1}\sum_{s=0}^{N-1} h_{p,t}h_{k,s}^*\phi_{\tilde{y}}(\omega)e^{i(s-t)\omega}d\omega \\
&= \frac{1}{2\pi}\int_{-\pi}^{\pi} H_p(\omega)H_k^*(\omega)\phi_{\tilde{y}}(\omega)d\omega \\
&\simeq \phi_{\tilde{y}}(0)h_p^*\left[\frac{1}{2\pi}\int_{-\beta\pi}^{\beta\pi} a(\omega)a^*(\omega)d\omega\right]h_k \\
&= \phi_y(\tilde{\omega})h_p^*\Gamma h_k = 0 \qquad \text{for } k \neq p
\end{aligned} \tag{5.3.27}$$

Thus, the random variables x_p and x_k (for $p \neq k$) are approximately uncorrelated under the assumptions made. This implies, at least under the assumption that the $\{x_k\}$ are Gaussian, that $|x_p|^2$ and $|x_k|^2$ are *statistically independent* (for $p \neq k$).

According to the calculations above, $\{|x_p|^2\}_{p=1}^K$ can approximately be considered to be independent random variables all with the same mean $\phi_y(\tilde{\omega})$. Then, we can estimate $\phi_y(\tilde{\omega})$ by the following average of $\{|x_p|^2\}$: $\frac{1}{K}\sum_{p=1}^K |x_p|^2$, or

$$\boxed{\hat{\phi}(\omega) = \frac{1}{K}\sum_{p=1}^{K}\left|\sum_{t=1}^{N} h_{p,N-t}y(t)e^{-i\omega t}\right|^2} \tag{5.3.28}$$

We may suspect that the random variables $\{|x_p|^2\}$ have not only the same mean, but also the same variance (this can, in fact, be readily shown under the Gaussian hypothesis). Whenever this is true, the variance of the average in (5.3.28) is K times smaller than the variance of each of the variables averaged. The above findings are summarized in the following.

If the resolution threshold β is increased K times from $\beta = 1/N$ (the lowest value) to $\beta = K/N$, then the variance of the RFB estimate in (5.3.22) may be reduced by a factor K by constructing the spectral estimate as in (5.3.28), where the pth baseband filter's impulse response $\{h_{p,t}\}_{t=0}^{N-1}$ is given by the pth dominant Slepian sequence ($p = 1, \ldots, K$). (5.3.29)

The RFB spectral estimator (5.3.28) can be given two interpretations. First, arguments similar with those following equation (5.3.22) suggest that *for large N the RFB estimate (5.3.28) behaves similarly to the Daniell method of periodogram averaging*. For small or medium–sized values of N, the RFB and Daniell methods behave differently. In such a case, we can relate (5.3.28) to the class of *multiwindow spectral estimators* [THOMSON 1982]. Indeed, the RFB estimate (5.3.28) can be interpreted as the average of K windowed periodograms, where the pth periodogram is computed from the raw data sequence $\{y(t)\}$ windowed with the pth dominant Slepian sequence. Note that since the Slepian sequences are given by the eigenvectors of the real *Toeplitz* matrix Γ, they must be either symmetric: $h_{p,N-t} = h_{p,t-1}$; or skew–symmetric: $h_{p,N-t} = -h_{p,t-1}$ (see Result R25 in Appendix A). This means that (5.3.28) can alternatively be written as

$$\hat{\phi}(\omega) = \frac{1}{K} \sum_{p=1}^{K} \left| \sum_{t=1}^{N} h_{p,t-1} y(t) e^{-i\omega t} \right|^2 \tag{5.3.30}$$

This form of the RFB estimate makes its interpretation as a multiwindow spectrum estimator more direct.

For a second interpretation of the RFB estimate (5.3.28), consider the follow-

ing (Daniell–type) spectrally smoothed periodogram estimator of $\phi(\tilde{\omega})$:

$$\begin{aligned}
\hat{\phi}(\tilde{\omega}) &= \frac{1}{2\pi\beta}\int_{\tilde{\omega}-\beta\pi}^{\tilde{\omega}+\beta\pi}\hat{\phi}_p(\omega)d\omega = \frac{1}{2\pi\beta}\int_{-\beta\pi}^{\beta\pi}\hat{\phi}_p(\omega+\tilde{\omega})d\omega \\
&= \frac{1}{2\pi\beta}\int_{-\beta\pi}^{\beta\pi}\frac{1}{N}\left|\sum_{t=1}^{N}y(t)e^{-i(\omega+\tilde{\omega})t}\right|^2 d\omega \\
&= \frac{1}{2\pi K}\int_{-\beta\pi}^{\beta\pi}\sum_{t=1}^{N}\sum_{s=1}^{N}\tilde{y}(t)\tilde{y}^*(s)e^{-i\omega t}e^{i\omega s}d\omega \\
&= \frac{1}{K}[\tilde{y}^*(1)\ \ldots\ \tilde{y}^*(N)] \\
&\quad \cdot\left\{\frac{1}{2\pi}\int_{-\beta\pi}^{\beta\pi}\begin{bmatrix}1\\ e^{i\omega}\\ \vdots\\ e^{i(N-1)\omega}\end{bmatrix}[1\ \ e^{-i\omega}\ldots e^{-i(N-1)\omega}]d\omega\right\}\begin{bmatrix}\tilde{y}(1)\\ \vdots\\ \tilde{y}(N)\end{bmatrix} \\
&= \frac{1}{K}[\tilde{y}^*(1)\ \ldots\ \tilde{y}^*(N)]\Gamma\begin{bmatrix}\tilde{y}(1)\\ \vdots\\ \tilde{y}(N)\end{bmatrix}
\end{aligned} \tag{5.3.31}$$

where we made use of the fact that Γ is real–valued. It follows from the result (5.3.15) that Γ can be approximated by the *rank–K* matrix:

$$\Gamma \simeq \sum_{p=1}^{K} s_p s_p^T = \sum_{p=1}^{K} h_p h_p^T \tag{5.3.32}$$

Inserting (5.3.32) into (5.3.31) and using the fact that the Slepian sequences $s_p = h_p$ are real–valued leads to the following PSD estimator:

$$\hat{\phi}(\tilde{\omega}) \simeq \frac{1}{K}\sum_{p=1}^{K}\left|\sum_{t=1}^{N}h_{p,t-1}\tilde{y}(t)\right|^2 \tag{5.3.33}$$

which is precisely the RFB estimator (5.3.30). Hence, the RFB estimate of the PSD can also be interpreted as a *reduced–rank smoothed periodogram*.

We might think of using the full–rank smoothed periodogram (5.3.31) as an estimator for PSD, in lieu of the reduced–rank smoothed periodogram (5.3.33) which coincides with the RFB estimate. However, from a theoretical standpoint we have no strong reason to do so. Moreover, from a practical standpoint we have clear reasons against such an idea. We can explain this briefly as follows. The K dominant eigenvectors of Γ can be *precomputed* with satisfactory numerical accuracy. Then, evaluation of (5.3.33) can be done by using an FFT algorithm in approximately $\frac{1}{2}KN\log_2 N = \frac{1}{2}\beta N^2\log_2 N$ flops. On the other hand, a direct evaluation of (5.3.31) would require N^2 flops for each value of ω, which leads to a prohibitively large total computational burden. A computationally efficient evaluation of (5.3.31) would require some factorization of Γ to be performed, such as the

eigendecomposition of Γ. However, Γ is an extremely ill–conditioned matrix (recall that $N-K=N(1-\beta)$ of its eigenvalues are close to zero), which means that such a complete factorization cannot easily be performed with satisfactory numerical accuracy. In any case even if we were able to precompute the eigendecomposition of Γ, evaluation of (5.3.31) would require $\frac{1}{2}N^2\log_2 N$ flops, which is still larger by a factor of $1/\beta$ than what is required for (5.3.33).

5.4 CAPON METHOD

The periodogram was previously shown to be a filter bank approach which uses a bandpass filter whose impulse response vector is given by the standard Fourier transform vector (*i.e.*, $[1, e^{-i\tilde{\omega}}, \ldots, e^{-i(N-1)\tilde{\omega}}]^T$). In the periodogram approach there is *no attempt to purposely design* the bandpass filter to achieve some desired characteristics (see, however, Section 5.5). The RFB method, on the other hand, uses a bandpass filter specifically designed to be "*as selective as possible*" *for a white noise input* (see (5.3.5) and the discussion preceding it). The RFB's filter is still *data independent* in the sense that it does not adapt to the processed data in any way. Presumably, it might be valuable to take the data properties into consideration when designing the bandpass filter. In other words, the filter should be designed to be "as selective as possible" (according to a criterion to be specified) not for a fictitious white noise input, but for the input consisting of the studied data themselves. This is the basic idea behind the Capon method, which is an FBA procedure based on a *data–dependent bandpass filter* [Capon 1969; Lacoss 1971].

5.4.1 Derivation of the Capon Method

The Capon method (CM), in contrast to the RFB estimator (5.3.28), uses only *one bandpass filter* for computing one estimated spectrum value. This suggests that if the CM is to provide statistically stable spectral estimates, then it should make use of the other approach which affords this: *splitting the raw sample into subsequences* and averaging the results obtained from each subsequence. Indeed, as we shall see the Capon method is essentially based on this second approach.

Consider a filter with a finite impulse response of length m, denoted by

$$h = [h_0 \;\; h_1 \ldots h_m]^* \tag{5.4.1}$$

where m is a positive integer that is unspecified for the moment. The output of the filter at time t, when the input is the raw data sequence $\{y(t)\}$, is given by

$$\begin{aligned} y_F(t) &= \sum_{k=0}^{m} h_k y(t-k) \\ &= h^* \begin{bmatrix} y(t) \\ y(t-1) \\ \vdots \\ y(t-m) \end{bmatrix} \end{aligned} \tag{5.4.2}$$

Let R denote the covariance matrix of the data vector in (5.4.2). Then the power

of the filter output can be written as:

$$E\left\{|y_F(t)|^2\right\} = h^* R h \tag{5.4.3}$$

where, according to the definition above,

$$R = E\left\{ \begin{bmatrix} y(t) \\ \vdots \\ y(t-m) \end{bmatrix} [y^*(t) \dots y^*(t-m)] \right\} \tag{5.4.4}$$

The response of the filter (5.4.2) to a sinusoidal component of frequency ω (say) is determined by the filter's frequency response:

$$H(\omega) = \sum_{k=0}^{m} h_k e^{-i\omega k} = h^* a(\omega) \tag{5.4.5}$$

where

$$a(\omega) = [1 \quad e^{-i\omega} \dots e^{-im\omega}]^T \tag{5.4.6}$$

If we want to make the filter as selective as possible for a frequency band around the current value ω, then we may think of minimizing the total power in (5.4.3) subject to the constraint that the filter passes the frequency ω undistorted. This idea leads to the following optimization problem:

$$\boxed{\min_h h^* R h \quad \text{subject to } h^* a(\omega) = 1} \tag{5.4.7}$$

The solution to (5.4.7) is given in Result R35 in Appendix A:

$$\boxed{h = R^{-1} a(\omega) / a^*(\omega) R^{-1} a(\omega)} \tag{5.4.8}$$

Inserting (5.4.8) into (5.4.3) gives

$$E\left\{|y_F(t)|^2\right\} = 1/a^*(\omega) R^{-1} a(\omega) \tag{5.4.9}$$

This is the power of $y(t)$ in a passband centered on ω. Then, assuming that the (idealized) conditions (i) and (ii) in (5.1.5) hold, we can approximately determine the value of the PSD of $y(t)$ at the passband's center frequency as

$$\phi(\omega) \simeq \frac{E\left\{|y_F(t)|^2\right\}}{\beta} = \frac{1}{\beta a^*(\omega) R^{-1} a(\omega)} \tag{5.4.10}$$

where β denotes the frequency bandwidth of the filter given by (5.4.8). The division by β, as above, is sometimes omitted in the literature, but it is required to complete the FBA scheme in Figure 5.1. Note that since the bandpass filter (5.4.8) is data dependent, its bandwidth β is not necessarily data independent, nor is it necessarily frequency independent. Hence, the division by β in (5.4.10) may not represent a

simple scaling of $E\left\{|y_F(t)|^2\right\}$, but it may change the shape of this quantity as a function of ω.

There are various possibilities for determining the bandwidth β, depending on the degree of precision we are aiming for. The simplest possibility is to set

$$\beta = 1/(m+1) \tag{5.4.11}$$

This choice is motivated by the time–bandwidth product result (2.6.5), which says that for a filter whose temporal aperture is equal to $(m+1)$, the bandwidth should roughly be given by $1/(m+1)$. By inserting (5.4.11) in (5.4.10), we obtain

$$\phi(\omega) \simeq \frac{(m+1)}{a^*(\omega)R^{-1}a(\omega)} \tag{5.4.12}$$

Note that if $y(t)$ is white noise of variance σ^2, (5.4.12) takes the correct value: $\phi(\omega) = \sigma^2$. In the general case, however, (5.4.11) gives only a rough indication of the filter's bandwidth, as the time–bandwidth product result does not apply exactly to the present situation (see the conditions under which (2.6.5) has been derived).

An often more exact expression for β can be obtained as follows [Lagunas, Santamaria, Gasull, and Moreno 1986]. The (equivalent) bandwidth of a bandpass filter can be defined as the support of the rectangle centered on ω (the filter's center frequency) that concentrates the whole energy in the filter's frequency response. According to this definition, β can be assumed to satisfy:

$$\int_{-\pi}^{\pi} |H(\psi)|^2 d\psi = |H(\omega)|^2 2\pi\beta \tag{5.4.13}$$

Since in the present case $H(\omega) = 1$ (see (5.4.7)), we obtain from (5.4.13):

$$\beta = \frac{1}{2\pi}\int_{-\pi}^{\pi} |h^* a(\psi)|^2 d\psi = h^* \left[\frac{1}{2\pi}\int_{-\pi}^{\pi} a(\psi)a^*(\psi)d\psi\right] h \tag{5.4.14}$$

The (k,p) element of the central matrix in the above quadratic form is given by

$$\frac{1}{2\pi}\int_{-\pi}^{\pi} e^{-i\psi(k-p)}d\psi = \delta_{k,p} \tag{5.4.15}$$

With this observation and (5.4.8), (5.4.14) leads to

$$\beta = h^*h = \frac{a^*(\omega)R^{-2}a(\omega)}{[a^*(\omega)R^{-1}a(\omega)]^2} \tag{5.4.16}$$

Note that this expression of the bandwidth is both data and frequency dependent (as was alluded to previously). Inserting (5.4.16) in (5.4.10) gives

$$\phi(\omega) \simeq \frac{a^*(\omega)R^{-1}a(\omega)}{a^*(\omega)R^{-2}a(\omega)} \tag{5.4.17}$$

Remark: The expression for β in (5.4.16) is based on the assumption that most of the area under the curve of $|H(\psi)|^2 = |h^*a(\psi)|^2$ (for $\psi \in [-\pi, \pi]$) is located

around the center frequency ω. This assumption is often true, but not always true. For instance, consider a data sequence $\{y(t)\}$ consisting of a number of sinusoidal components with frequencies $\{\omega_k\}$ in noise with *small* power. Then the Capon filter (5.4.8) with center frequency ω will likely place nulls at $\{\psi = \omega_k\}$ to annihilate the strong sinusoidal components in the data, but will pay little attention to the weak noise component. The consequence is that $|H(\psi)|^2$ will be nearly zero at $\{\psi = \omega_k\}$, and one at $\psi = \omega$ (by (5.4.7)), but may take rather large values at other frequencies (see, for example, the numerical examples in [LI AND STOICA 1996A], which demonstrate this behavior of the Capon filter). In such a case, the formula (5.4.16) may significantly overestimate the "true" bandwidth, and hence the spectral formula (5.4.17) may significantly underestimate the PSD $\phi(\omega)$. ■

In the derivations above, the true data covariance matrix R has been assumed available. In order to turn the previous PSD formulas into practical spectral estimation algorithms, we must replace R in these formulas by a sample estimate, for instance by

$$\hat{R} = \frac{1}{N-m} \sum_{t=m+1}^{N} \begin{bmatrix} y(t) \\ \vdots \\ y(t-m) \end{bmatrix} [y^*(t) \dots y^*(t-m)] \tag{5.4.18}$$

Doing so, we obtain the following two spectral estimators corresponding to (5.4.12) and (5.4.17), respectively:

$$\boxed{\text{CM–Version 1:} \quad \hat{\phi}(\omega) = \frac{m+1}{a^*(\omega)\hat{R}^{-1}a(\omega)}} \tag{5.4.19}$$

$$\boxed{\text{CM–Version 2:} \quad \hat{\phi}(\omega) = \frac{a^*(\omega)\hat{R}^{-1}a(\omega)}{a^*(\omega)\hat{R}^{-2}a(\omega)}} \tag{5.4.20}$$

There is an implicit assumption in both (5.4.19) and (5.4.20) that $\hat{R}^{-1}$ exists. This assumption sets a limit on the maximum value that can be chosen for m:

$$\boxed{m < N/2} \tag{5.4.21}$$

(Observe that $\text{rank}(\hat{R}) \leq N - m$, which is less than $\dim(\hat{R}) = m + 1$ if (5.4.21) is violated.) The inequality (5.4.21) is important since it sets a limit on the resolution achievable by the Capon method. Indeed, since the Capon method is based on a bandpass filter with impulse response's aperture equal to m, we may expect its resolution threshold to be on the order of $1/m > 2/N$ (with the inequality following from (5.4.21)).

As m is decreased, we can expect the resolution of Capon method to become worse (*cf.* the previous discussion). On the other hand, the accuracy with which $\hat{R}$ is determined increases with decreasing m (since more outer products are averaged

in (5.4.18)). The main consequence of the increased accuracy of $\hat{R}$ is to statistically stabilize the spectral estimate (5.4.19) or (5.4.20). Hence, the choice of m should be done with the ubiquitous tradeoff between resolution and statistical accuracy in mind. It is interesting to note that for the Capon method both the filter design and power calculation stages are data dependent. The accuracy of both these stages may worsen if m is chosen too large. In applications, the maximum value that can be chosen for m might also be limited from considerations of computational complexity.

Empirical studies have shown that *the ability of the Capon method to resolve fine details of a PSD, such as closely spaced peaks, is superior to the corresponding performance of the periodogram–based methods*. This superiority may be attributed to the higher statistical stability of Capon method, as explained next. For m smaller than $N/2$ (see (5.4.21)), we may expect the Capon method to possess worse resolution but better statistical accuracy compared with the unwindowed or "mildly windowed" periodogram method. It should be stressed that *the notion of "resolution" refers to the ability of the theoretically averaged spectral estimate* $E\{\hat{\phi}(\omega)\}$ *to resolve fine details in the true PSD* $\phi(\omega)$. This resolution is roughly inversely proportional to the window's length or the bandpass filter impulse response's aperture. *The "resolving power" corresponding to the estimate* $\hat{\phi}(\omega)$ *is more difficult to quantify*, but — of course — it is what interests the most. It should be clear that the resolving power of $\hat{\phi}(\omega)$ depends not only on the bias of this estimate (*i.e.*, on $E\{\hat{\phi}(\omega)\}$), but also on its variance. *A spectral estimator with low bias–based resolution but high statistical accuracy may be better able to resolve finer details in a studied PSD than can a high resolution/low accuracy estimator*. Since the periodogram may achieve better bias–based resolution than the Capon method, the higher (empirically observed) "resolving power" of the latter should be due to a better statistical accuracy (*i.e.*, a lower variance).

In the context of the previous discussion, it is interesting to note that the Blackman–Tukey periodogram with a Bartlett window of length $2m+1$, which is given by (see (2.5.1)):

$$\hat{\phi}_{\mathrm{BT}}(\omega) = \sum_{k=-m}^{m} \frac{(m+1-|k|)}{m+1} \hat{r}(k) e^{-i\omega k}$$

can be written in a form that bears some resemblance with the form (5.4.19) of the CM–Version 1 estimator. A straightforward calculation gives

$$\hat{\phi}_{\mathrm{BT}}(\omega) = \sum_{t=0}^{m} \sum_{s=0}^{m} \hat{r}(t-s) e^{-i\omega(t-s)} / (m+1) \tag{5.4.22}$$

$$= \frac{1}{m+1} a^*(\omega) \hat{R} a(\omega) \tag{5.4.23}$$

where $a(\omega)$ is as defined in (5.4.6), and $\hat{R}$ is the Hermitian Toeplitz sample covari-

ance matrix

$$\hat{R} = \begin{bmatrix} \hat{r}(0) & \hat{r}(1) & \dots & \hat{r}(m) \\ \hat{r}^*(1) & \hat{r}(0) & \ddots & \vdots \\ \vdots & \ddots & \ddots & \hat{r}(1) \\ \hat{r}^*(m) & \dots & \hat{r}^*(1) & \hat{r}(0) \end{bmatrix}$$

Comparing the above expression for $\hat{\phi}_{\mathrm{BT}}(\omega)$ with (5.4.19), it is seen that the *CM–Version 1 can be obtained from Blackman–Tukey estimator by replacing* $\hat{R}$ *in the Blackman–Tukey estimator with* $\hat{R}^{-1}$*, and then inverting the so–obtained quadratic form.* Below we provide a brief explanation as to why this replacement and inversion make sense. That is, if we ignore for a moment the technically sound filter bank derivation of the Capon method, then why should the above way of obtaining CM–Version 1 from the Blackman–Tukey method provide a reasonable spectral estimator? We begin by noting that (*cf.* Section 1.3.2):

$$\lim_{m\to\infty} E\left\{ \frac{1}{m+1} \left| \sum_{t=0}^{m} y(t) e^{-i\omega t} \right|^2 \right\} = \phi(\omega)$$

However, a simple calculation shows that

$$E\left\{ \frac{1}{m+1} \left| \sum_{t=0}^{m} y(t) e^{-i\omega t} \right|^2 \right\} = \frac{1}{m+1} \sum_{t=0}^{m} \sum_{s=0}^{m} r(t-s) e^{-i\omega t} e^{i\omega s} = \frac{1}{m+1} a^*(\omega) R a(\omega)$$

Hence,

$$\lim_{m\to\infty} \frac{1}{m+1} a^*(\omega) R a(\omega) = \phi(\omega) \tag{5.4.24}$$

Similarly, one can show that

$$\lim_{m\to\infty} \frac{1}{m+1} a^*(\omega) R^{-1} a(\omega) = \phi^{-1}(\omega) \tag{5.4.25}$$

(see, *e.g.*, [Hannan and Wahlberg 1989]). Comparing (5.4.24) with (5.4.25) provides the explanation we were looking for. Observe that the CM–Version 1 estimator is a finite–sample approximation to equation (5.4.25), whereas the Blackman–Tukey estimator is a finite–sample approximation to equation (5.4.24).

The Capon method has also been compared with the AR method of spectral estimation (see Section 3.2). It has been empirically observed that *the CM–Version 1 possesses less variance but worse resolution than the AR spectral estimator.* This may be explained by making use of the relationship that exists between the CM–Version 1 and AR spectral estimators; see the next subsection (and also [Burg 1972]). The CM–Version 2 spectral estimator is less well studied and hence its properties are not so well understood. In the following subsection, we also relate the CM–Version 2 to the AR spectral estimator. In the case of CM–Version 2, the relationship is more involved, hence leaving less room for intuitive explanations.

5.4.2 Relationship between Capon and AR Methods

The AR method of spectral estimation has been described in Chapter 3. In the following we consider the covariance matrix estimate in (5.4.18). The AR method corresponding to this sample covariance matrix is the LS method discussed in Section 3.4.2. Let us denote the matrix $\hat{R}$ in (5.4.18) by $\hat{R}_{m+1}$ and its principal lower–right $k \times k$ block by $\hat{R}_k$ $(k = 1, \ldots, m+1)$, as shown below:

$\hat{R} \;=$

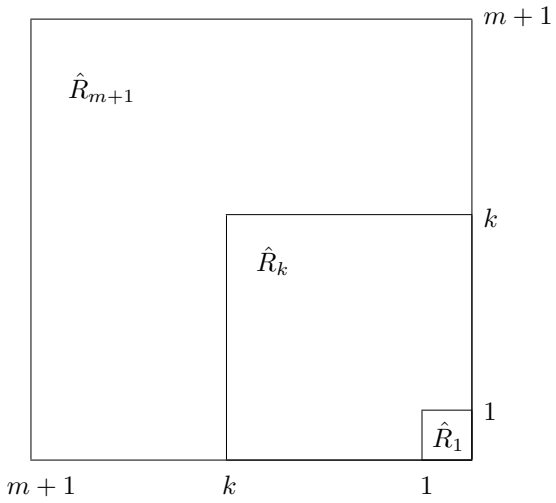

(5.4.26)

With this notation, the coefficient vector θ_k and the residual power σ_k^2 of the *kth–order AR model* fitted to the data $\{y(t)\}$ are obtained as the solutions to the following matrix equation (refer to (3.4.6)):

$$\hat{R}_{k+1} \begin{bmatrix} 1 \\ \hat{\theta}_k^c \end{bmatrix} = \begin{bmatrix} \hat{\sigma}_k^2 \\ 0 \end{bmatrix} \tag{5.4.27}$$

(the complex conjugate in (5.4.27) appears owing to the fact that $\hat{R}_k$ above is equal to the complex conjugate of the sample covariance matrix used in Chapter 3). The nested structure of (5.4.26) along with the defining equation (5.4.27) imply:

$$\hat{R}_{m+1} \begin{bmatrix} 1 & 0 & \ldots & 0 & 0 \\ & 1 & & \vdots & \vdots \\ & & \ddots & 0 & \\ & & & 1 & 0 \\ \hat{\theta}_m^c & \hat{\theta}_{m-1}^c & & \hat{\theta}_1^c & 1 \end{bmatrix} = \begin{bmatrix} \hat{\sigma}_m^2 & x & \ldots & x \\ 0 & \hat{\sigma}_{m-1}^2 & \ddots & \vdots \\ \vdots & \ddots & \ddots & x \\ 0 & \cdots & 0 & \hat{\sigma}_0^2 \end{bmatrix} \tag{5.4.28}$$

where "x" stands for undetermined elements. Let

$$\hat{\mathcal{H}} = \begin{bmatrix} 1 & 0 & \dots & 0 & 0 \\ & 1 & & \vdots & \vdots \\ & & \ddots & 0 & \\ & & & 1 & 0 \\ \hat{\theta}_m^c & \hat{\theta}_{m-1}^c & & \hat{\theta}_1^c & 1 \end{bmatrix} \tag{5.4.29}$$

It follows from (5.4.28) that

$$\hat{\mathcal{H}}^* \hat{R}_{m+1} \hat{\mathcal{H}} = \begin{bmatrix} \hat{\sigma}_m^2 & x & \dots & x \\ & \hat{\sigma}_{m-1}^2 & \ddots & \vdots \\ 0 & & \ddots & x \\ & & & \hat{\sigma}_0^2 \end{bmatrix} \tag{5.4.30}$$

(where, once more, x denotes undetermined elements). Since $\hat{\mathcal{H}}^* \hat{R}_{m+1} \hat{\mathcal{H}}$ is a Hermitian matrix, the elements designated by "x" in (5.4.30) must be equal to zero. Hence, we have proven the following result which is essential in establishing a relation between the AR and Capon methods of spectral estimation (this result extends the one in Exercise 3.7 to the non–Toeplitz covariance case).

The parameters $\{\hat{\theta}_k, \hat{\sigma}_k^2\}$ of the AR models of orders $k = 1, 2, \dots, m$ determine the following factorization of the inverse (sample) covariance matrix:

$$\hat{R}_{m+1}^{-1} = \hat{\mathcal{H}} \hat{\Sigma}^{-1} \hat{\mathcal{H}}^* \quad ; \quad \hat{\Sigma} = \begin{bmatrix} \hat{\sigma}_m^2 & & & 0 \\ & \hat{\sigma}_{m-1}^2 & & \\ & & \ddots & \\ 0 & & & \hat{\sigma}_0^2 \end{bmatrix} \tag{5.4.31}$$

Let

$$\hat{A}_k(\omega) = [1 \;\; e^{-i\omega} \dots e^{-ik\omega}] \begin{bmatrix} 1 \\ \hat{\theta}_k \end{bmatrix} \tag{5.4.32}$$

denote the polynomial corresponding to the kth–order AR model, and let

$$\hat{\phi}_k^{\mathrm{AR}}(\omega) = \frac{\hat{\sigma}_k^2}{|\hat{A}_k(\omega)|^2} \tag{5.4.33}$$

denote its associated PSD (see Chapter 3). It is readily verified that

$$\begin{aligned} a^*(\omega)\hat{\mathcal{H}} &= [1 \;\; e^{i\omega} \dots e^{im\omega}] \begin{bmatrix} 1 & 0 & \dots & 0 & 0 \\ & 1 & & \vdots & \vdots \\ & & \ddots & 0 & \\ & & & 1 & 0 \\ \hat{\theta}_m^c & \hat{\theta}_{m-1}^c & & \hat{\theta}_1^c & 1 \end{bmatrix} \\ &= [\hat{A}_m^*(\omega), \; e^{i\omega}\hat{A}_{m-1}^*(\omega), \; \dots, \; e^{im\omega}\hat{A}_0^*(\omega)] \end{aligned} \tag{5.4.34}$$

It follows from (5.4.31) and (5.4.34) that the quadratic form in the denominator of the CM–Version 1 spectral estimator can be written as

$$\begin{aligned} a^*(\omega)\hat{R}^{-1}a(\omega) &= a^*(\omega)\hat{\mathcal{H}}\hat{\Sigma}^{-1}\hat{\mathcal{H}}^*a(\omega) \\ &= \sum_{k=0}^{m} |\hat{A}_k(\omega)|^2/\hat{\sigma}_k^2 = \sum_{k=0}^{m} 1/\hat{\phi}_k^{\mathrm{AR}}(\omega) \end{aligned} \tag{5.4.35}$$

which leads at once to the following result:

$$\boxed{\hat{\phi}_{\text{CM–1}}(\omega) = \frac{1}{\dfrac{1}{m+1}\displaystyle\sum_{k=0}^{m} 1/\hat{\phi}_k^{\mathrm{AR}}(\omega)}} \tag{5.4.36}$$

This is the desired relation between the CM–Version 1 and the AR spectral estimates. This relation says that the inverse of the CM–Version 1 spectral estimator can be obtained by averaging the inverse estimated AR spectra of orders from 0 to m. In view of the averaging operation in (5.4.36), it is not difficult to understand why the CM–Version 1 possesses less statistical variability than the AR estimator. Moreover, the fact that the CM–Version 1 has also been found to have worse resolution and bias properties than the AR spectral estimate should be due to the presence of low–order AR models in (5.4.36).

Next, consider the CM–Version 2. The previous analysis of CM–Version 1 already provides a relation between the numerator in the spectral estimate corresponding to CM–Version 2, (5.4.20), and the AR spectra. In order to obtain a similar expression for the denominator in (5.4.20), some preparations are required. The (sample) covariance matrix $\hat{R}$ can be used to define $m+1$ *AR models of order* m, depending on which coefficient of the AR equation

$$\hat{a}_0 y(t) + \hat{a}_1 y(t-1) + \ldots + \hat{a}_m y(t-m) = \text{residuals} \tag{5.4.37}$$

we choose to set to one. The AR model $\{\hat{\theta}_m, \hat{\sigma}_m^2\}$ used in the previous analysis corresponds to setting $\hat{a}_0 = 1$ in (5.4.37). However, in principle, any other AR coefficient in (5.4.37) may be normalized to one. The mth–order LS AR model obtained by setting $\hat{a}_k = 1$ in (5.4.37) is denoted by $\{\hat{\mu}_k =$ coefficient vector and $\hat{\gamma}_k =$ residual variance$\}$, and is given by the solution to the following linear system of equations (compare with (5.4.27)):

$$\hat{R}_{m+1}\hat{\mu}_k^c = \hat{\gamma}_k u_k \tag{5.4.38}$$

where the $(k+1)$st component of $\hat{\mu}_k$ is equal to one $(k = 0, \ldots, m)$, and where u_k stands for the $(k+1)$st column of the $(m+1) \times (m+1)$ identity matrix:

$$u_k = [\underbrace{0 \ldots 0}_{k} \quad 1 \quad \underbrace{0 \ldots 0}_{m-k}]^T \tag{5.4.39}$$

Evidently, $[1\ \hat{\theta}_m^T]^T = \hat{\mu}_0$ and $\hat{\sigma}_m^2 = \hat{\gamma}_0$.

Similarly to (5.4.32) and (5.4.33), the (estimated) PSD corresponding to the kth mth–order AR model given by (5.4.38) is obtained as

$$\hat{\phi}_k^{\mathrm{AR}(m)}(\omega) = \frac{\hat{\gamma}_k}{|a^*(\omega)\hat{\mu}_k^c|^2} \tag{5.4.40}$$

It is shown in the following calculation that the denominator in (5.4.20) can be expressed as a (weighted) average of the AR spectra in (5.4.40):

$$\begin{aligned}\sum_{k=0}^{m} \frac{1}{\hat{\gamma}_k \hat{\phi}_k^{\mathrm{AR}(m)}(\omega)} &= \sum_{k=0}^{m} \frac{|a^*(\omega)\hat{\mu}_k^c|^2}{\hat{\gamma}_k^2} = a^*(\omega) \left[\sum_{k=0}^{m} \frac{\hat{\mu}_k^c \hat{\mu}_k^T}{\hat{\gamma}_k^2} \right] a(\omega) \\ &= a^*(\omega)\hat{R}^{-1} \left[\sum_{k=0}^{m} u_k u_k^* \right] \hat{R}^{-1} a(\omega) = a^*(\omega)\hat{R}^{-2} a(\omega)\end{aligned} \tag{5.4.41}$$

Combining (5.4.35) and (5.4.41) gives

$$\hat{\phi}_{\mathrm{CM–2}}\ (\omega) = \frac{\sum_{k=0}^{m} 1/\hat{\phi}_k^{\mathrm{AR}}(\omega)}{\sum_{k=0}^{m} 1/\hat{\gamma}_k \hat{\phi}_k^{\mathrm{AR}(m)}(\omega)} \tag{5.4.42}$$

The above relation appears to be more involved, and hence more difficult to interpret, than the similar relation (5.4.36) corresponding to CM–Version 1. Nevertheless, since (5.4.42) is still obtained by averaging various AR spectra, we may expect that *the CM–Version 2 estimator, like the CM–Version 1 estimator, is more statistically stable but has poorer resolution than the AR spectral estimator.*

5.5 FILTER BANK REINTERPRETATION OF THE PERIODOGRAM

As we saw in Section 5.2, the basic periodogram spectral estimator can be interpreted as an FBA method with a *preimposed* bandpass filter (whose impulse response is equal to the Fourier transform vector). In contrast, RFB and Capon are FBA methods based on *designed* bandpass filters. The filter used in the RFB method is data independent, whereas it is a function of the data covariances in the Capon method. The use of a data–dependent bandpass filter, such as in the Capon method, is intuitively appealing but it also leads to the following drawback: since we need to consistently estimate the filter impulse response, the temporal aperture of the filter should be chosen (much) smaller than the sample length, which sets a rather hard limit on the achievable spectral resolution. In addition, it appears that any other filter design methodology, except the one originally suggested by Capon, will most likely lead to a problem (such as an eigenanalysis) that should be solved for each value of the center frequency; which — of course — would be a rather prohibitive computational task. With these difficulties of the data–dependent design in mind, we may content ourselves with a "well–designed" data–independent filter. The purpose of this section is to show that *the basic periodogram and the Daniell method can be interpreted as FBA methods based on well–designed data–independent filters*, similar to the RFB method. As we will see, the bandpass filters

used by the aforementioned periodogram methods are obtained *by combining the design procedures employed in the RFB and Capon methods*.

The following result is required (see R35 in Appendix A for a proof). Let R, H, A and C be matrices of dimensions $(m \times m)$, $(m \times K)$, $(m \times n)$ and $(K \times n)$, respectively. Assume that R is positive definite and A has full column rank equal to n (hence, $m \geq n$). Then the solution to the following quadratic optimization problem with linear constraints:

$$\min_H (H^* R H) \quad \text{subject to} \quad H^* A = C$$

is given by

$$H = R^{-1} A (A^* R^{-1} A)^{-1} C^* \tag{5.5.1}$$

We can now proceed to derive our "new" FBA–based spectral estimation method (as we will see below, it turns out that this method is not really new!). We would like this method to possess a facility for compromising between the bias and variance of the estimated PSD. As explained in the previous sections of this chapter, there are two main ways of doing this within the FBA: we either (i) use a bandpass filter with temporal aperture less than N, obtain the allowed number of samples of the filtered signal and then calculate the power from these samples; or (ii) use a set of K bandpass filters with length–N impulse responses, that cover a band centered on the current frequency value, obtain one sample of the filtered signals for each filter in the set and calculate the power by averaging these K samples. As argued in Section 5.3, approach (ii) may be more effective than (i) in reducing the variance of the estimated PSD, while keeping the bias low. In the sequel, we follow approach (ii).

Let $\beta \geq 1/N$ be the *prespecified (desired) resolution* and let K be defined by equation (5.3.12): $K = \beta N$. According to the time–bandwidth product result, a bandpass filter with a length–N impulse response may be expected to have a bandwidth on the order of $1/N$ (but not less). Hence, we can cover the preimposed passband

$$[\tilde{\omega} - \beta\pi, \tilde{\omega} + \beta\pi] \tag{5.5.2}$$

(here $\tilde{\omega}$ stands for the current frequency value) by using $2\pi\beta/(2\pi/N) = K$ filters, which pass essentially nonoverlapping $1/N$–length frequency bands in the interval (5.5.2). *The requirement that the filters' passbands are (nearly) nonoverlapping is a key condition for variance reduction.* In order to see this, let x_p denote the sample obtained at the output of the pth filter:

$$x_p = \sum_{k=0}^{N-1} h_{p,k} y(N-k) = \sum_{t=1}^{N} h_{p,N-t} y(t) \tag{5.5.3}$$

Here $\{h_{p,k}\}_{k=0}^{N-1}$ is the pth filter's impulse response. The associated frequency response is denoted by $H_p(\omega)$. Note that in the present case we consider bandpass filters operating on the raw data, in lieu of baseband filters operating on demodulated data (as in RFB). Assume that the *center–frequency gain* of each filter is normalized so that

$$H_p(\tilde{\omega}) = 1, \qquad p = 1, \ldots, K \tag{5.5.4}$$

Then, we can write

$$E\left\{|x_p|^2\right\} = \frac{1}{2\pi}\int_{-\pi}^{\pi}|H_p(\omega)|^2\phi(\omega)d\omega$$
$$\simeq \frac{1}{2\pi}\int_{\tilde{\omega}-\pi/N}^{\tilde{\omega}+\pi/N}\phi(\omega)d\omega \simeq \frac{2\pi/N}{2\pi}\phi(\tilde{\omega}) = \frac{1}{N}\phi(\tilde{\omega}) \tag{5.5.5}$$

The second "equality" in (5.5.5) follows from (5.5.4) and the *assumed bandpass characteristics of* $H_p(\omega)$, and the third equality results from the assumption that $\phi(\omega)$ *is approximately constant over the passband*. (Note that the angular frequency passband of $H_p(\omega)$ is $2\pi/N$, as explained before.) In view of (5.5.5), we can estimate $\phi(\tilde{\omega})$ by averaging over the squared magnitudes of the filtered samples $\{x_p\}_{p=1}^{K}$. By doing so, we may achieve a reduction in variance by a factor K, *provided* $\{x_p\}$ are statistically independent (see Section 5.3 for details). Under the assumption that the filters $\{H_p(\omega)\}$ pass essentially nonoverlapping frequency bands, we readily get (compare (5.3.27)):

$$E\{x_p x_k^*\} = \frac{1}{2\pi}\int_{-\pi}^{\pi}H_p(\omega)H_k^*(\omega)\phi(\omega)d\omega \simeq 0 \tag{5.5.6}$$

which implies that the random variables $\{|x_p|^2\}$ are independent at least under the Gaussian hypothesis. Without the previous assumption on $\{H_p(\omega)\}$, the filtered samples $\{x_p\}$ may be strongly correlated and, therefore, a reduction in variance by a factor K cannot be guaranteed.

The conclusion from the previous (more or less heuristic) discussion is summarized in the following.

> If the passbands of the filters used to cover the prespecified interval (5.5.2) do not overlap, then by using all filters' output samples — as contrasted to using the output sample of only one filter — we achieve a reduction in the variance of the estimated PSD by a factor equal to the number of filters. The maximum number of such filters that can be found is given by $K = \beta N$. (5.5.7)

By using the insights provided by the above discussion, as summarized in (5.5.7), we can now approach the bandpass filters design problem. We sample the frequency axis as in the FFT (as almost any practical implementation of a spectral estimation method does):

$$\tilde{\omega}_s = \frac{2\pi}{N}s \qquad s = 0, \ldots, N-1 \tag{5.5.8}$$

The frequency samples that fall within the passband (5.5.2) are readily seen to be the following:

$$\frac{2\pi}{N}(s+p) \qquad p = -K/2, \ldots, 0, \ldots, K/2-1 \tag{5.5.9}$$

(to simplify the discussion we assume that K is an even integer). Let

$$H = [h_1 \ldots h_K] \qquad (N \times K) \tag{5.5.10}$$

denote the matrix whose pth column is equal to the impulse response vector corresponding to the pth bandpass filter. We assume that *the input to the filters is white noise (as in RFB) and design the filters so as to minimize the output power under the constraint that each filter passes undistorted one (and only one) of the frequencies in (5.5.9) (as in Capon).* These design objectives lead to the following optimization problem:

$$\boxed{\begin{array}{c}\min_H(H^*H) \text{ subject to } H^*A = I \\ \text{where } A = \left[a\left(\frac{2\pi}{N}\left(s-\frac{K}{2}\right)\right),\ldots,a\left(\frac{2\pi}{N}\left(s+\frac{K}{2}-1\right)\right)\right]\end{array}} \tag{5.5.11}$$

and where $a(\omega) = [1 \quad e^{-i\omega} \ldots e^{-i(N-1)\omega}]^T$. Note that the constraint in (5.5.11) guarantees that each frequency in the passband (5.5.9) is passed undistorted by one filter in the set, and it is annihilated by all the other $(K-1)$ filters. In particular, observe that (5.5.11) implies (5.5.4).

The solution to (5.5.11) follows at once from the result (5.5.1): the minimizing H matrix is given by

$$H = A(A^*A)^{-1} \tag{5.5.12}$$

However, the columns in A are orthogonal

$$A^*A = NI$$

(see (4.3.15)); therefore, (5.5.12) simplifies to

$$\boxed{H = \frac{1}{N}A} \tag{5.5.13}$$

which is the solution of the filter design problem previously formulated.

By using (5.5.13) in (5.5.3), we get

$$\begin{aligned}|x_p|^2 &= \frac{1}{N^2}\left|\sum_{t=1}^{N} e^{i(N-t)\frac{2\pi}{N}(s+p)}y(t)\right|^2 \\ &= \frac{1}{N^2}\left|\sum_{t=1}^{N} y(t)e^{-i\frac{2\pi}{N}(s+p)t}\right|^2 \\ &= \frac{1}{N}\hat{\phi}_p\left(\frac{2\pi}{N}(s+p)\right) \qquad p = -K/2,\ldots,K/2-1\end{aligned} \tag{5.5.14}$$

where the dependence of $|x_p|^2$ on s (and hence on $\tilde{\omega}_s$) is omitted to simplify the notation, and where $\hat{\phi}_p(\omega)$ is the standard periodogram. Finally, (5.5.14) along with (5.5.5) lead to the following *FBA spectral estimator*:

$$\boxed{\hat{\phi}\left(\frac{2\pi}{N}s\right) = \frac{1}{K}\sum_{p=-K/2}^{K/2-1} N|x_p|^2 = \frac{1}{K}\sum_{l=s-K/2}^{s+K/2-1}\hat{\phi}_p\left(\frac{2\pi}{N}l\right)} \tag{5.5.15}$$

which coincides with the Daniell periodogram estimator (2.7.16). Furthermore, *for* $K = 1$ (*i.e.*, $\beta = 1/N$, which is the choice suitable for "high–resolution" applications), *(5.5.15) reduces to the unmodified periodogram.* Recall also that the RFB method in Section 5.3, for large data lengths, is expected to have similar performance to the Daniell method for $K > 1$ and to the basic periodogram for $K = 1$. Hence, in the family of nonparametric spectral estimation methods the periodograms "are doing well".

5.6 COMPLEMENTS

5.6.1 Another Relationship between the Capon and AR Methods

The relationship between the AR and Capon spectra established in Section 5.4.2 involves all AR spectral models of orders 0 through m. Another interesting relationship, which involves the AR spectrum of order m alone, is presented in this complement.

Let $\hat{\theta} = [\hat{a}_0\ \hat{a}_1 \dots \hat{a}_m]^T$ (with $\hat{a}_0 = 1$) denote the vector of the coefficients of the mth–order AR model fitted to the data sample covariances, and let $\hat{\sigma}^2$ denote the corresponding residual variance (see Chapter 3 and (5.4.27)). Then the mth–order AR spectrum is given by:

$$\hat{\phi}_{AR}(\omega) = \frac{\hat{\sigma}^2}{|a^*(\omega)\hat{\theta}^c|^2} = \frac{\hat{\sigma}^2}{|\sum_{k=0}^{m}\ \hat{a}_k e^{-i\omega k}|^2} \tag{5.6.1}$$

By a simple calculation, $\hat{\phi}_{AR}(\omega)$ above can be rewritten in the following form:

$$\boxed{\hat{\phi}_{AR}(\omega) = \frac{\hat{\sigma}^2}{\sum_{s=-m}^{m}\ \hat{\rho}(s)e^{i\omega s}}} \tag{5.6.2}$$

where

$$\boxed{\hat{\rho}(s) = \sum_{k=0}^{m-s} \hat{a}_k \hat{a}_{k+s}^* = \hat{\rho}^*(-s), \qquad s = 0, \dots, m.} \tag{5.6.3}$$

To show this, note that

$$\left|\sum_{k=0}^{m}\ \hat{a}_k e^{-i\omega k}\right|^2 = \sum_{k=0}^{m}\sum_{p=0}^{m} \hat{a}_k \hat{a}_p^* e^{-i\omega(k-p)} = \sum_{k=0}^{m}\sum_{s=k-m}^{k} \hat{a}_k \hat{a}_{k-s}^* e^{-i\omega s}$$

$$= \sum_{k=0}^{m}\sum_{s=-m}^{m} \hat{a}_k \hat{a}_{k-s}^* e^{-i\omega s} = \sum_{s=-m}^{m}\sum_{k=0}^{m} \hat{a}_k \hat{a}_{k+s}^* e^{i\omega s}$$

$$= \sum_{s=-m}^{m} \left(\sum_{k=0}^{m-s} \hat{a}_k \hat{a}_{k+s}^*\right)\ e^{i\omega s}$$

and (5.6.2)–(5.6.3) immediately follows.

Next, assume that the (sample) covariance matrix $\hat{R}$ is Toeplitz. (We note in passing that this is a minor restriction for the temporal spectral estimation problem of this chapter, but it may be quite a restrictive assumption for the spatial problem of the next chapter.) Then the Capon spectrum in equation (5.4.19) (with the factor $m+1$ omitted, for convenience) can be written as:

$$\boxed{\hat{\phi}_{CM}(\omega) = \frac{\hat{\sigma}^2}{\sum_{s=-m}^{m} \hat{\mu}(s) e^{i\omega s}}} \tag{5.6.4}$$

where

$$\boxed{\hat{\mu}(s) = \sum_{k=0}^{m-s} (m+1-2k-s)\hat{a}_k \hat{a}_{k+s}^* = \hat{\mu}^*(-s), \qquad s = 0, \ldots, m} \tag{5.6.5}$$

To prove (5.6.4) we make use of the Gohberg–Semencul (GS) formula derived in Complement 3.9.4, which is repeated here for convenience:

$$\hat{\sigma}^2 \hat{R}^{-1} = \begin{bmatrix} 1 & \cdots & \cdots & 0 \\ \hat{a}_1^* & \ddots & & \vdots \\ \vdots & \ddots & \ddots & \vdots \\ \hat{a}_m^* & \cdots & \hat{a}_1^* & 1 \end{bmatrix} \begin{bmatrix} 1 & \hat{a}_1 & \cdots & \hat{a}_m \\ \vdots & \ddots & \ddots & \vdots \\ \vdots & & \ddots & \hat{a}_1 \\ 0 & \cdots & \cdots & 1 \end{bmatrix}$$

$$- \begin{bmatrix} 0 & \cdots & \cdots & 0 \\ \hat{a}_m & \ddots & & \vdots \\ \vdots & \ddots & \ddots & \vdots \\ \hat{a}_1 & \cdots & \hat{a}_m & 0 \end{bmatrix} \begin{bmatrix} 0 & \hat{a}_m^* & \cdots & \hat{a}_1^* \\ \vdots & \ddots & \ddots & \vdots \\ \vdots & & \ddots & \hat{a}_m^* \\ 0 & \cdots & \cdots & 0 \end{bmatrix}$$

(The above formula is in fact the complex conjugate of the GS formula in Complement 3.9.4 because the matrix $\hat{R}$ above is the complex conjugate of the one considered in Chapter 3).

For the sake of convenience, let $\hat{a}_k = 0$ for $k \notin [0,\ m]$. By making use of this convention, and of the GS formula, we obtain:

$$\begin{aligned} f(\omega) &\triangleq \hat{\sigma}^2 a^*(\omega) \hat{R}^{-1} a(\omega) \\ &= \sum_{p=0}^{m} \left\{ \left| \sum_{k=0}^{m} \hat{a}_{k-p}\ e^{-i\omega k} \right|^2 - \left| \sum_{k=0}^{m} \hat{a}_{m+1-k+p}^* e^{-i\omega k} \right|^2 \right\} \\ &= \sum_{p=0}^{m} \sum_{k=0}^{m} \sum_{\ell=0}^{m} (\hat{a}_{k-p} \hat{a}_{\ell-p}^* - \hat{a}_{m+1+p-k}^* \hat{a}_{m+1-\ell+p}) e^{i\omega(\ell-k)} \\ &= \sum_{\ell=0}^{m} \sum_{p=0}^{m} \sum_{s=\ell-m}^{\ell} (\hat{a}_{\ell-s-p} \hat{a}_{\ell-p}^* - \hat{a}_{m+1-\ell+s+p}^* \hat{a}_{m+1+p-\ell}) e^{i\omega s} \end{aligned} \tag{5.6.6}$$

where the last equality has been obtained by the substitution $s = \ell - k$. Next, make the substitution $j = \ell - p$ in (5.6.6) to obtain:

$$f(\omega) = \sum_{\ell=0}^{m} \sum_{j=\ell-m}^{\ell} \sum_{s=\ell-m}^{\ell} (\hat{a}_{j-s}\hat{a}_j^* - \hat{a}_{m+1-j}\hat{a}_{m+1+s-j}^*)e^{i\omega s} \tag{5.6.7}$$

Since $\hat{a}_{j-s} = 0$ and $\hat{a}_{m+1+s-j}^* = 0$ for $s > j$, we can extend the summation over s in (5.6.7) up to $s = m$. Furthermore, the summand in (5.6.7) is zero for $j < 0$, and hence we can truncate the summation over j to the interval $[0,\ \ell]$. These two observations yield:

$$f(\omega) = \sum_{\ell=0}^{m} \sum_{j=0}^{\ell} \sum_{s=\ell-m}^{m} (\hat{a}_{j-s}\hat{a}_j^* - \hat{a}_{m+1-j}\hat{a}_{m+1+s-j}^*)e^{i\omega s} \tag{5.6.8}$$

Next, decompose $f(\omega)$ additively as follows:

$$f(\omega) = T_1(\omega) + T_2(\omega)$$

where

$$T_1(\omega) = \sum_{\ell=0}^{m} \sum_{j=0}^{\ell} \sum_{s=0}^{m} (\hat{a}_{j-s}\hat{a}_j^* - \hat{a}_{m+1-j}\hat{a}_{m+1+s-j}^*)e^{i\omega s}$$

$$T_2(\omega) = \sum_{\ell=0}^{m} \sum_{j=0}^{\ell} \sum_{s=\ell-m}^{-1} (\hat{a}_{j-s}\hat{a}_j^* - \hat{a}_{m+1-j}\hat{a}_{m+1+s-j}^*)e^{i\omega s}$$

(The term in T_2 corresponding to $\ell = m$ is zero.) Let

$$\hat{\mu}(s) \triangleq \sum_{\ell=0}^{m} \sum_{j=0}^{\ell} (\hat{a}_{j-s}\hat{a}_j^* - \hat{a}_{m+1-j}\hat{a}_{m+1+s-j}^*) \tag{5.6.9}$$

By using this notation, we can write $T_1(\omega)$ as

$$T_1(\omega) = \sum_{s=0}^{m} \hat{\mu}(s)e^{i\omega s}$$

Since $f(\omega)$ is real–valued for any $\omega \in [-\pi,\ \pi]$, we must also have

$$T_2(\omega) = \sum_{s=-1}^{-m} \hat{\mu}^*(-s)e^{i\omega s}$$

As the summand in (5.6.9) does not depend on ℓ, we readily obtain

$$\hat{\mu}(s) = \sum_{j=0}^{m} (m+1-j)\ (\hat{a}_{j-s}\hat{a}_j^* - \hat{a}_{m+1-j}\hat{a}_{m+1+s-j}^*)$$

$$= \sum_{k=0}^{m-s} (m+1-k-s)\ \hat{a}_k\hat{a}_{k+s}^* - \sum_{k=1}^{m} k\hat{a}_k\hat{a}_{k+s}^*$$

$$= \sum_{k=0}^{m-s} (m+1-2k-s)\hat{a}_k\hat{a}_{k+s}^*$$

which coincides with (5.6.5). Thus, the proof of (5.6.4) is concluded.

Remark: The reader may wonder what happens with the formulas derived above if the AR model parameters are calculated by using the same sample covariance matrix as in the Capon estimator. In such a case, the parameters $\{\hat{a}_k\}$ in (5.6.1) and in the GS formula above should be replaced by $\{\hat{a}_k^*\}$ (see (5.4.27)). Consequently both (5.6.2)–(5.6.3) and (5.6.4)–(5.6.5) continue to hold but with $\{\hat{a}_k\}$ replaced by $\{\hat{a}_k^*\}$ (and $\{\hat{a}_k^*\}$ replaced by $\{\hat{a}_k\}$, of course). ■

By comparing (5.6.2) and (5.6.4) we see that the reciprocals of both $\hat{\phi}_{AR}(\omega)$ and $\hat{\phi}_{CM}(\omega)$ have the form of a Blackman–Tukey spectral estimate associated with the "covariance sequences" $\{\hat{\rho}(s)\}$ and $\{\hat{\mu}(s)\}$, respectively. The only difference between $\hat{\phi}_{AR}(\omega)$ and $\hat{\phi}_{CM}(\omega)$ is that the sequence $\{\hat{\mu}(s)\}$ corresponding to $\hat{\phi}_{CM}(\omega)$ is a "linearly tapered" version of the sequence $\{\hat{\rho}(s)\}$ corresponding to $\hat{\phi}_{AR}(\omega)$. Similar to the interpretation in Section 5.4.2, the previous observation can be used to intuitively understand why the Capon spectral estimates are smoother and have poorer resolution than the AR estimates of the same order. (For more details on this aspect and other aspects related to the discussion in this complement, see [Musicus 1985].)

We remark in passing that the name "covariance sequence" given, for example, to $\{\hat{\rho}(s)\}$ is not coincidental: $\{\hat{\rho}(s)\}$ are so–called *sample inverse covariances* associated with $\hat{R}$ and they can be shown to possess a number of interesting and useful properties (see, *e.g.*, [Cleveland 1972; Bhansali 1980]).

The formula (5.6.4) can be used for the computation of $\hat{\phi}_{CM}(\omega)$, as we now show. Assuming that $\hat{R}$ is already available, we can use the Levinson–Durbin algorithm to compute $\{\hat{a}_k\}$ and $\hat{\sigma}^2$, and then $\{\hat{\mu}(s)\}$ in $\mathcal{O}(m^2)$ flops. Then (5.6.4) can be evaluated at M Fourier frequencies (say) by using the FFT. The resulting total computational burden is on the order of $\mathcal{O}(m^2 + M \log_2 M)$ flops. For commonly encountered values of m and M, this is about m times smaller than the burden associated with the eigendecomposition–based computational procedure of Exercise 5.5. Note, however, that the latter algorithm can be applied to a general $\hat{R}$ matrix, whereas the one derived in this complement is limited to Toeplitz covariance matrices. Finally, note that the extension of the results in this complement to two–dimensional (2D) signals can be found in [Jakobsson, Marple, and Stoica 2000].

5.6.2 Multiwindow Interpretation of Daniell and Blackman–Tukey Periodograms

As stated in Exercise 5.1, the Bartlett and Welch periodograms can be cast into the multiwindow framework of Section 5.3.3. In other words, they can be written in the following form (see (5.7.1))

$$\hat{\phi}(\omega) = \frac{1}{K} \sum_{p=1}^{K} \left| \sum_{t=1}^{N} w_{p,t}\, y(t) e^{-i\omega t} \right|^2 \tag{5.6.10}$$

for certain temporal (or data) windows $\{w_{p,t}\}$ (also called *tapers*). Here, K denotes the number of windows used by the method in question.

In this complement we show that the Daniell periodogram, as well as the Blackman–Tukey periodogram with some commonly-used lag windows, can also be interpreted as multiwindow methods. Unlike the approximate multiwindow interpretation of a spectrally smoothed periodogram described in Section 5.3.3 (see equations (5.3.31)–(5.3.33) there), the multiwindow interpretations presented in this complement are *exact*. More details on the topic of this complement can be found in [McCloud, Scharf, and Mullis 1999], where it is also shown that the Blackman–Tukey periodogram with any "good" window can be cast in a multiwindow framework, but only approximately.

We begin by writing (5.6.10) as a quadratic form in the data sequence. Let

$$z(\omega) = \begin{bmatrix} y(1)e^{-i\omega} \\ \vdots \\ y(N)e^{-iN\omega} \end{bmatrix}, \qquad (N \times 1)$$

$$W = \begin{bmatrix} w_{1,1} & \cdots & w_{1,N} \\ \vdots & & \vdots \\ w_{K,1} & \cdots & w_{K,N} \end{bmatrix}, \qquad (K \times N)$$

and let $[x]_p$ denote the pth element of a vector x. Using this notation we can rewrite (5.6.10) in the desired form:

$$\hat{\phi}(\omega) = \frac{1}{K} \sum_{p=1}^{K} \left| [Wz(\omega)]_p \right|^2$$

or

$$\boxed{\hat{\phi}(\omega) = \frac{1}{K} z^*(\omega) W^* W z(\omega)} \qquad (5.6.11)$$

which is a quadratic form in $z(\omega)$. The rank of the matrix W^*W is less than or equal to K; typically, $\text{rank}(W^*W) = K \ll N$.

Next we turn our attention to the Daniell periodogram (see (2.7.16)):

$$\hat{\phi}_D(\omega) = \frac{1}{2J+1} \sum_{j=-J}^{J} \hat{\phi}_p\left(\omega + j\frac{2\pi}{N}\right) \qquad (5.6.12)$$

where $\hat{\phi}_p(\omega)$ is the standard periodogram given in (2.2.1):

$$\hat{\phi}_p(\omega) = \frac{1}{N} \left| \sum_{t=1}^{N} y(t) e^{-i\omega t} \right|^2$$

Letting

$$a_j^* = \left[e^{-i\frac{2\pi}{N}j}, e^{-i\frac{2\pi}{N}(2j)}, \ldots, e^{-i\frac{2\pi}{N}(Nj)} \right] \qquad (5.6.13)$$

we can write

$$\hat{\phi}_p\left(\omega + j\frac{2\pi}{N}\right) = \frac{1}{N}\left|\sum_{t=1}^{N} y(t)e^{-i\omega t}e^{-i\frac{2\pi}{N}(jt)}\right|^2$$
$$= \frac{1}{N}\left|a_j^* z(\omega)\right|^2 = \frac{1}{N} z^*(\omega)a_j a_j^* z(\omega) \tag{5.6.14}$$

which implies that

$$\boxed{\hat{\phi}_D(\omega) = \frac{1}{N(2J+1)} z^*(\omega)W_D^* W_D z(\omega)} \tag{5.6.15}$$

where

$$\boxed{W_D = [a_{-J}, \ldots, a_0, \ldots, a_J]^*, \qquad (2J+1) \times N} \tag{5.6.16}$$

This establishes the fact that *the Daniell periodogram can be interpreted as a multiwindow method using* $K = 2J+1$ *tapers given by* (5.6.16). Similarly to the tapers used by the seemingly more elaborate RFB approach, the Daniell periodogram tapers can also be motivated using a sound design methodology (see Section 5.5).

In the remaining part of this complement we consider the Blackman–Tukey periodogram in (2.5.1) with a window of length $M = N$:

$$\hat{\phi}_{BT}(\omega) = \sum_{k=-(N-1)}^{N-1} w(k)\hat{r}(k)e^{-i\omega k} \tag{5.6.17}$$

A commonly-used class of windows, including the Hanning and Hamming windows in Table 2.1, is described by the equation:

$$w(k) = \alpha + \beta\cos(\Delta k) = \left(\alpha + \tfrac{\beta}{2}e^{i\Delta k} + \tfrac{\beta}{2}e^{-i\Delta k}\right) \tag{5.6.18}$$

for various parameters α, β, and Δ. Inserting (5.6.18) into (5.6.17) yields:

$$\hat{\phi}_{BT}(\omega) = \sum_{k=-(N-1)}^{N-1} \left(\alpha + \tfrac{\beta}{2}e^{i\Delta k} + \tfrac{\beta}{2}e^{-i\Delta k}\right)\hat{r}(k)e^{-i\omega k}$$
$$= \alpha\hat{\phi}_p(\omega) + \tfrac{\beta}{2}\hat{\phi}_p(\omega - \Delta) + \tfrac{\beta}{2}\hat{\phi}_p(\omega + \Delta) \tag{5.6.19}$$

where $\hat{\phi}_p(\omega)$ is the standard periodogram given by (2.2.1) or, equivalently, by (2.2.2):

$$\hat{\phi}_p(\omega) = \sum_{k=-(N-1)}^{N-1} \hat{r}(k)e^{-i\omega k}$$

Comparing (5.6.19) with (5.6.12) (as well as (5.6.14)–(5.6.16)) allows us to rewrite $\hat{\phi}_{BT}(\omega)$ in the following form:

$$\boxed{\hat{\phi}_{BT}(\omega) = \frac{1}{N} z^*(\omega)W_{BT}^* W_{BT} z(\omega)} \tag{5.6.20}$$

where

$$W_{BT} = \left[\sqrt{\tfrac{\beta}{2}}a_{-\Delta}, \sqrt{\alpha}a_0, \sqrt{\tfrac{\beta}{2}}a_{\Delta}\right]^*, \qquad (3 \times N) \tag{5.6.21}$$

for $\alpha, \beta \geq 0$ and where a_Δ is given by (similarly to a_j in (5.6.13))

$$a_\Delta^* = \left[e^{-i\Delta}, \ldots, e^{-i\Delta N}\right]$$

Hence, we conclude that *the Blackman–Tukey periodogram with a Hamming or Hanning window (or any other window having the form of (5.6.18)) can be interpreted as a multiwindow method using $K = 3$ tapers given by (5.6.21).* Similarly, $\hat{\phi}_{BT}(\omega)$ using the Blackman window in Table 2.1 can be shown to be equivalent to a multiwindow method with $K = 7$ tapers.

Interestingly, as a byproduct of the analysis in this complement, we note from (5.6.19) that the Blackman–Tukey periodogram with a window of the form in (5.6.18) can be *very efficiently* computed from the values of the standard periodogram. Since the Blackman window has a form similar to (5.6.18), $\hat{\phi}_{BT}(\omega)$ using the Blackman window can be similarly implemented in an efficient way. This way of computing $\hat{\phi}_{BT}(\omega)$ is faster than the method outlined in Complement 2.8.2 for a general lag window.

5.6.3 Capon Method for Exponentially Damped Sinusoidal Signals

The signals which are dealt with in some applications of spectral analysis, such as in magnetic resonance spectroscopy, consist of a sum of *exponentially damped sinusoidal components*, (or damped sinusoids, for short), instead of the pure sinusoids as in (4.1.1). Such signals are described by the equation

$$y(t) = \sum_{k=1}^{n} \beta_k e^{(\rho_k + i\omega_k)t} + e(t), \qquad t = 1, \ldots, N \tag{5.6.22}$$

where β_k and ω_k are the amplitude and frequency of the kth component (as in Chapter 4), and $\rho_k < 0$ is the so-called damping parameter. The (noise-free) signal in (5.6.22) is *nonstationary* and hence it does not have a power spectral density. However, it possesses an *amplitude spectrum* that is defined as follows:

$$|\beta(\rho, \omega)| = \begin{cases} |\beta_k|, & \text{for } \omega = \omega_k, \rho = \rho_k \quad (k = 1, \ldots, n) \\ 0, & \text{elsewhere} \end{cases} \tag{5.6.23}$$

Furthermore, because an exponentially damped sinusoid satisfies the finite energy condition in (1.2.1), the (noise-free) signal in (5.6.22) also possesses an *energy spectrum*. Similarly to (5.6.23), we can define the energy spectrum of the damped sinusoidal signal in (5.6.22) as a 2D function of (ρ, ω) that consists of n pulses at $\{\rho_k, \omega_k\}$, where the height of the function at each of these points is equal to the energy of the corresponding component. The energy of a generic component with parameters (β, ρ, ω) is given by

$$\sum_{t=1}^{N} \left|\beta e^{(\rho + i\omega)t}\right|^2 = |\beta|^2 e^{2\rho} \sum_{t=0}^{N-1} e^{2\rho t} = |\beta|^2 e^{2\rho} \frac{1 - e^{2\rho N}}{1 - e^{2\rho}} \tag{5.6.24}$$

It follows from (5.6.24) and the above discussion that the energy spectrum can be expressed as a function of the amplitude spectrum in (5.6.23) via the formula:

$$E(\rho,\omega) = |\beta(\rho,\omega)|^2 L(\rho) \tag{5.6.25}$$

where

$$L(\rho) = e^{2\rho}\frac{1-e^{2\rho N}}{1-e^{2\rho}} \tag{5.6.26}$$

The amplitude spectrum, and hence the energy spectrum, of the signal in (5.6.22) can be estimated by using *an extension of the Capon method* that is introduced in Section 5.4. To develop this extension, we consider the following data vector

$$\tilde{y}(t) = [y(t), y(t+1), \ldots, y(t+m)] \tag{5.6.27}$$

in lieu of the data vector used in (5.4.2). First we explain why, in the case of damped sinusoidal signals, the use of (5.6.27) is preferable to that of

$$[y(t), y(t-1), \ldots, y(t-m)]^T \tag{5.6.28}$$

(as is used in (5.4.2)). Let h denote the coefficient vector of the Capon FIR filter as in (5.4.1). Then, the output of the filter using the data vector in (5.6.27) is given by:

$$\tilde{y}_F(t) = h^*\tilde{y}(t) = h^*\begin{bmatrix} y(t) \\ \vdots \\ y(t+m) \end{bmatrix}, \qquad t = 1, \ldots, N-m \tag{5.6.29}$$

Hence, when performing the filtering operation as in (5.6.29), we lose m samples from the end of the data string. Because the SNR of those samples is typically rather low (owing to the damping of the signal components), the data loss is not significant. In contrast, the use of (5.4.2) leads to a loss of m data samples from the beginning of the data string (since (5.4.2) can be computed for $t = m+1, \ldots, N$), where the SNR is higher. Hence, in the case of damped sinusoidal signals we should indeed prefer (5.6.29) to (5.4.2).

Next, we derive Capon-like estimates of the amplitude and energy spectra of (5.6.22). Let

$$\hat{R} = \frac{1}{N-m}\sum_{t=1}^{N-m} \tilde{y}(t)\tilde{y}^*(t) \tag{5.6.30}$$

denote the sample covariance matrix of the data vector in (5.6.27). Then the sample variance of the filter output can be written as:

$$\frac{1}{N-m}\sum_{t=1}^{N-m} |\tilde{y}_F(t)|^2 = h^*\hat{R}h \tag{5.6.31}$$

By definition, the Capon filter minimizes (5.6.31) under the constraint that the filter passes, without distortion, a generic damped sinusoid with parameters (β, ρ, ω).

The filter output corresponding to such a generic component is given by

$$h^* \begin{bmatrix} \beta e^{(\rho+i\omega)t} \\ \beta e^{(\rho+i\omega)(t+1)} \\ \vdots \\ \beta e^{(\rho+i\omega)(t+m)} \end{bmatrix} = \left(h^* \begin{bmatrix} 1 \\ e^{\rho+i\omega} \\ \vdots \\ e^{(\rho+i\omega)m} \end{bmatrix} \right) \beta e^{(\rho+i\omega)t} \tag{5.6.32}$$

Hence, the distortionless filtering constraint can be expressed as

$$h^* a(\rho, \omega) = 1 \tag{5.6.33}$$

where

$$\boxed{a(\rho, \omega) = \left[1, e^{\rho+i\omega}, \ldots, e^{(\rho+i\omega)m}\right]^T} \tag{5.6.34}$$

The minimizer of the quadratic function in (5.6.31) under the linear constraint (5.6.33) is given by the familiar formula (see (5.4.7)–(5.4.8)):

$$\boxed{h(\rho, \omega) = \frac{\hat{R}^{-1} a(\rho, \omega)}{a^*(\rho, \omega) \hat{R}^{-1} a(\rho, \omega)}} \tag{5.6.35}$$

where we have stressed, via notation, the dependence of h on both ρ and ω.

The output of the filter in (5.6.35) due to a possible (generic) damped sinusoid in the signal with parameters (β, ρ, ω), is given by (*cf.* (5.6.32) or (5.6.33)):

$$h^*(\rho, \omega) \tilde{y}(t) = \beta e^{(\rho+i\omega)t} + e_F(t), \qquad t = 1, \ldots, N-m \tag{5.6.36}$$

where $e_F(t)$ denotes the filter output due to noise and to any other signal components. For given (ρ, ω), the least-squares estimate of β in (5.6.36) is (see, *e.g.*, Result R32 in Appendix A):

$$\hat{\beta}(\rho, \omega) = \frac{\sum_{t=1}^{N-m} h^*(\rho, \omega) \tilde{y}(t) e^{(\rho-i\omega)t}}{\sum_{t=1}^{N-m} e^{2\rho t}} \tag{5.6.37}$$

Let $\tilde{L}(\rho)$ be defined similarly to $L(\rho)$ in (5.6.26), but with N replaced by $N-m$, and let

$$\boxed{\tilde{Y}(\rho, \omega) = \frac{1}{\tilde{L}(\rho)} \sum_{t=1}^{N-m} \tilde{y}(t) e^{(\rho-i\omega)t}} \tag{5.6.38}$$

It follows from (5.6.37), along with (5.6.25), that Capon-like estimates of the amplitude spectrum and energy spectrum of the signal in (5.6.22) can be obtained,

respectively, as:

$$\boxed{\left|\hat{\beta}(\rho,\omega)\right| = \left|h^*(\rho,\omega)\tilde{Y}(\rho,\omega)\right|} \tag{5.6.39}$$

and

$$\boxed{\hat{E}(\rho,\omega) = \left|\hat{\beta}(\rho,\omega)\right|^2 L(\rho)} \tag{5.6.40}$$

Remark: We could have estimated the amplitude, β, of a generic component with parameters (β,ρ,ω) directly from the unfiltered data samples $\{y(t)\}_{t=1}^{N}$. However, the use of the Capon filtered data in (5.6.36) usually leads to enhanced performance. The main reason for this performance gain lies in the fact that the SNR corresponding to the generic component in the filtered data is typically much higher than in the raw data, owing to the good rejection properties of the Capon filter. This higher SNR leads to more accurate amplitude estimates, in spite of the loss of m data samples in the filtering operation in (5.6.36). ■

Finally, we note that the sample Capon energy or amplitude spectrum can be used *to estimate the signal parameters* $\{\beta_k,\rho_k,\omega_k\}$ in a standard manner. Specifically, we compute either $|\hat{\beta}(\rho,\omega)|$ or $\hat{E}(\rho,\omega)$ at the points of a fine grid covering the region of interest in the two–dimensional (ρ,ω) plane, and obtain estimates of (ρ_k,ω_k) as the locations of the n largest spectral peaks; estimates of β_k can then be derived from (5.6.37) with (ρ,ω) replaced by the estimated values of (ρ_k,ω_k). There is empirical evidence that the use of $\hat{E}(\rho,\omega)$ in general leads to (slightly) more accurate signal parameter estimates than the use of $|\hat{\beta}(\rho,\omega)|$ (see [Stoica and Sundin 2001]). For more details on the topic of this complement, including the computation of the two–dimensional spectra in (5.6.39) and (5.6.40), we refer the reader to [Stoica and Sundin 2001].

5.6.4 Amplitude and Phase Estimation Method (APES)

The design idea behind the Capon filter is based on the following two principles, as discussed in Section 5.4:

(a) the sinusoid with frequency ω (currently considered in the analysis) passes through the filter in a distortionless manner; and

(b) any other frequencies in the data (corresponding, *e.g.*, to other sinusoidal components in the signal or to noise) are suppressed by the filter as much as possible.

The output of the filter whose input is a sinusoid with frequency ω, $\{\beta e^{i\omega t}\}$, is given by (assuming forward filtering, as in (5.4.2)):

$$h^* \begin{bmatrix} e^{i\omega t} \\ e^{i\omega(t-1)} \\ \vdots \\ e^{i\omega(t-m)} \end{bmatrix} \beta = \left(h^* \begin{bmatrix} 1 \\ e^{-i\omega} \\ \vdots \\ e^{-i\omega m} \end{bmatrix} \right) \beta e^{i\omega t} \tag{5.6.41}$$

For backward filtering, as used in Complement 5.6.3, a similar result can be derived. It follows from (5.6.41) that the design objective in (a) above can be expressed mathematically via the following linear constraint on h:

$$h^* a(\omega) = 1 \tag{5.6.42}$$

where

$$a(\omega) = \left[1, e^{-i\omega}, \ldots, e^{-i\omega m}\right]^T \tag{5.6.43}$$

(see (5.4.5)–(5.4.7)). Regarding the second design objective, its statement in (b) above is sufficiently general to allow several different mathematical formulations. The Capon method is based on the idea that the goal in (b) is achieved if the power at the filter output is minimized (see (5.4.7)). In this complement, another way to formulate (b) mathematically is described.

At a given frequency ω, let us choose h such that the filter output, $\{h^*\tilde{y}(t)\}$, where

$$\tilde{y}(t) = [y(t), y(t-1), \ldots, y(t-m)]^T$$

is as close as possible in a least-squares (LS) sense to a sinusoid with frequency ω and constant amplitude β. Mathematically, we obtain both h and β, for a given ω, by minimizing the LS criterion:

$$\boxed{\min_{h,\beta} \frac{1}{N-m} \sum_{t=m+1}^{N} \left|h^*\tilde{y}(t) - \beta e^{i\omega t}\right|^2 \quad \text{subject to } h^* a(\omega) = 1} \tag{5.6.44}$$

Note that the estimation of the amplitude and phase (*i.e.*, $|\beta|$ and $\arg(\beta)$) of the sinusoid with frequency ω is an intrinsic part of the method based on (5.6.44). This observation motives the name of *Amplitude and Phase EStimation* (APES) given to the method described by (5.6.44).

Because (5.6.44) is a linearly constrained quadratic problem, we should be able to find its solution in closed form. Let

$$\boxed{g(\omega) = \frac{1}{N-m} \sum_{t=m+1}^{N} \tilde{y}(t) e^{-i\omega t}} \tag{5.6.45}$$

Then, a straightforward calculation shows that the criterion function in (5.6.44) can be rewritten as:

$$\begin{aligned}
&\frac{1}{N-m} \sum_{t=m+1}^{N} \left|h^*\tilde{y}(t) - \beta e^{i\omega t}\right|^2 \\
&\quad = h^*\hat{R}h - \beta^* h^* g(\omega) - \beta g^*(\omega)h + |\beta|^2 \\
&\quad = \left|\beta - h^* g(\omega)\right|^2 + h^*\hat{R}h - \left|h^* g(\omega)\right|^2 \\
&\quad = \left|\beta - h^* g(\omega)\right|^2 + h^*\left[\hat{R} - g(\omega)g^*(\omega)\right]h
\end{aligned} \tag{5.6.46}$$

where

$$\hat{R} = \frac{1}{N-m} \sum_{t=m+1}^{N} \tilde{y}(t)\tilde{y}^*(t) \tag{5.6.47}$$

(see (5.4.18)). The minimization of (5.6.46) with respect to β is immediate:

$$\beta(\omega) = h^* g(\omega) \tag{5.6.48}$$

Inserting (5.6.48) into (5.6.46) yields the following problem whose solution will determine the filter coefficient vector:

$$\min_h h^* \hat{Q}(\omega) h \qquad \text{subject to } h^* a(\omega) = 1 \tag{5.6.49}$$

where

$$\hat{Q}(\omega) = \hat{R} - g(\omega) g^*(\omega) \tag{5.6.50}$$

As (5.6.49) has the same form as the Capon filter design problem (see (5.4.7)), the solution to (5.6.49) is readily derived (compare with (5.4.8)):

$$h(\omega) = \frac{\hat{Q}^{-1}(\omega) a(\omega)}{a^*(\omega) \hat{Q}^{-1}(\omega) a(\omega)} \tag{5.6.51}$$

A direct implementation of (5.6.51) would require the inversion of the matrix $\hat{Q}(\omega)$ for each value of $\omega \in [0, 2\pi]$ considered. To avoid such an intensive computational task, we can use the matrix inversion lemma (Result R27 in Appendix A) to express the inverse in (5.6.51) as follows:

$$\hat{Q}^{-1}(\omega) = \left[\hat{R} - g(\omega) g^*(\omega)\right]^{-1} = \hat{R}^{-1} + \frac{\hat{R}^{-1} g(\omega) g^*(\omega) \hat{R}^{-1}}{1 - g^*(\omega) \hat{R}^{-1} g(\omega)} \tag{5.6.52}$$

Inserting (5.6.52) into (5.6.51) yields the following expression for the *APES filter*:

$$\boxed{h(\omega) = \frac{\left[1 - g^*(\omega)\hat{R}^{-1}g(\omega)\right] \hat{R}^{-1} a(\omega) + \left[g^*(\omega)\hat{R}^{-1}a(\omega)\right] \hat{R}^{-1} g(\omega)}{\left[1 - g^*(\omega)\hat{R}^{-1}g(\omega)\right] a^*(\omega)\hat{R}^{-1}a(\omega) + \left|a^*(\omega)\hat{R}^{-1}g(\omega)\right|^2}} \tag{5.6.53}$$

From (5.6.48) and (5.6.53) we obtain the following formula for *the APES estimate of the (complex) amplitude spectrum* (see Complement 5.6.3 for a definition of the amplitude spectrum):

$$\boxed{\beta(\omega) = \frac{a^*(\omega)\hat{R}^{-1}g(\omega)}{\left[1 - g^*(\omega)\hat{R}^{-1}g(\omega)\right] a^*(\omega)\hat{R}^{-1}a(\omega) + \left|a^*(\omega)\hat{R}^{-1}g(\omega)\right|^2}} \tag{5.6.54}$$

Compared with the *Capon estimate of the amplitude spectrum* given by

$$\beta(\omega) = \frac{a^*(\omega)\hat{R}^{-1}g(\omega)}{a^*(\omega)\hat{R}^{-1}a(\omega)} \tag{5.6.55}$$

we see that the APES estimate in (5.6.54) is more computationally involved, but not by much.

Remark: Our discussion has focused on the estimation of the amplitude spectrum. If the power spectrum is what we want to estimate, then we can use the APES filter, (5.6.53), in the PSD estimation approach described in Section 5.4, or we can simply take $|\beta(\omega)|^2$ (along with a possible scaling) as an estimate of the PSD. ■

The above derivation of APES is adapted from [Stoica, Li, and Li 1999]. The original derivation of APES, provided in [Li and Stoica 1996a], was different: it was based on an approximate maximum likelihood approach. We refer the reader to [Li and Stoica 1996a] for the original derivation of APES as well as many other details on this approach to spectral analysis.

We end this complement with a brief comparison of Capon and APES from a performance standpoint. Extensive empirical and analytical studies of these two methods (see, *e.g.*, [Larsson, Li, and Stoica 2003] and its references) have shown that Capon has a (slightly) higher resolution than APES and also that the Capon estimates of the frequencies of a multicomponent sinusoidal signal in noise are more accurate than the APES estimates. On the other hand, for a given set of frequency estimates $\{\hat{\omega}_k\}$ in the vicinity of the true frequencies, the APES estimates of the amplitudes $\{\beta_k\}$ are much more accurate than the Capon estimates; the Capon estimates are always biased towards zero, sometimes significantly so. This suggests that, at least for spectral line analysis, a better method than both Capon and APES can be obtained by combining them in the following way:

- Estimate the frequencies $\{\omega_k\}$ as the locations of the dominant peaks of the Capon spectrum.
- Estimate the amplitudes $\{\beta_k\}$ using the APES formula (5.6.54) evaluated at the frequency estimates obtained in the previous step.

The above *combined Capon-APES (CAPES) method* was introduced in [Jakobsson and Stoica 2000].

5.6.5 Amplitude and Phase Estimation Method for Gapped Data (GAPES)

In some applications of spectral analysis the data sequence has gaps, owing to the failure of a measuring device, or owing to the impossibility to perform measurements for some periods of time (such as in astronomy). In this complement we will present an extension of the Amplitude and Phase EStimation (APES) method, outlined in Complement 5.6.4, to *gapped-data sequences*. Gapped-data sequences are evenly sampled data strings that contain unknown samples which are usually, but not always, clustered together in groups of reasonable size. We will use the acronym GAPES to designate the extended approach.

Most of the available methods for the spectral analysis of gapped data perform (either implicitly or explicitly) an interpolation of the missing data, followed by a standard full-data spectral analysis. The data interpolation step is critical and it cannot be completed without making (sometimes hidden) assumptions on the data sequence. For example, one such assumption is that the data is bandlimited with a

known cutoff frequency. Intuitively, these assumptions can be viewed as attempts to add extra "information" to the spectral analysis problem, which might be able to compensate for the lost information due to the missing data samples. The problem with these assumptions, though, is that they are not generally easy to check in applications, either *a priori* or *a posteriori*. The GAPES approach presented here is based on the sole assumption that *the spectral content of the missing data is similar to that of the available data*. This assumption is very natural, and one could argue that it introduces no restriction at all.

We begin the derivation of GAPES by rewriting the APES least-squares fitting criterion (see equation (5.6.44) in Complement 5.6.4) in a form that is more convenient for the discussion here. Specifically, we use the notation $h(\omega)$ and $\beta(\omega)$ to stress the dependence on ω of both the APES filter and the amplitude spectrum. Also, we note that in applications the frequency variable is usually sampled as follows:

$$\omega_k = \frac{2\pi}{K}k, \qquad k = 1, \ldots, K \tag{5.6.56}$$

where K is an integer (much) larger than N. Making use of the above notation and (5.6.56) we rewrite the APES criterion as follows:

$$\begin{aligned} \min \sum_{k=1}^{K} \sum_{t=m+1}^{N} & \left| h^*(\omega_k)\tilde{y}(t) - \beta(\omega_k)e^{i\omega_k t} \right|^2 \\ & \text{subject to } h^*(\omega_k)a(\omega_k) = 1 \text{ for } k = 1, \ldots, K \end{aligned} \tag{5.6.57}$$

Evidently, the minimization of the criterion in (5.6.57) with respect to $\{h(\omega_k)\}$ and $\{\beta(\omega_k)\}$ reduces to the minimization of the inner sum in (5.6.57) for each k. Hence, in the full-data case the problem in (5.6.57) is equivalent to the standard APES problem in equation (5.6.44) in Complement 5.6.4. However, in the gapped data case the form of the APES criterion in (5.6.57) turns out to be more convenient than that in (5.6.44), as we will see below.

To continue, we need some additional notation. Let

$$y_a = \text{the vector containing the available samples in } \{y(t)\}_{t=1}^{N}$$

$$y_u = \text{the vector containing the unavailable samples in } \{y(t)\}_{t=1}^{N}$$

The main idea behind the GAPES approach is to minimize (5.6.57) with respect to both $\{h(\omega_k)\}$ and $\{\beta(\omega_k)\}$ *as well as* with respect to y_u. Such a formulation of the gapped-data problem is appealing, because it leads to:

(i) an analysis filter bank $\{h(\omega_k)\}$ for which the filtered sequence is as close as possible in a LS sense to the (possible) sinusoidal component in the data that has frequency ω_k, which is the main design goal in the filter bank approach to spectral analysis; and

(ii) an estimate of the missing samples in y_u whose spectral content mimics the spectral content of the available data as much as possible in the LS sense of (5.6.57).

The criterion in (5.6.57) is a *quartic* function of the unknowns $\{h(\omega_k)\}$, $\{\beta(\omega_k)\}$, and y_u. Consequently, in general, its minimization requires the use of an iterative algorithm; that is, a closed-form solution is unlikely to exist. The GAPES method uses a *cyclic minimizer* to minimize the criterion in (5.6.57) (see Complement 4.9.5 for a general description of cyclic minimizers). A *step-by-step description of GAPES* is as follows:

The GAPES Algorithm

Step 0. Obtain initial estimates of $\{h(\omega_k)\}$ and $\{\beta(\omega_k)\}$.

Step 1. Use the most recent estimates of $\{h(\omega_k)\}$ and $\{\beta(\omega_k)\}$ to estimate y_u via the minimization of (5.6.57).

Step 2. Use the most recent estimate of y_u to estimate $\{h(\omega_k)\}$ and $\{\beta(\omega_k)\}$ via the minimization of (5.6.57).

Step 3. Check the convergence of the iteration, *e.g.*, by checking whether the relative change of the criterion between two consecutive iterations is smaller than a pre-assigned value. If *no*, then go to Step 1. If *yes*, then we have a final amplitude spectrum estimate given by $\{\hat{\beta}(\omega_k)\}_{k=1}^{K}$. If desired, this estimate can be transformed into a power spectrum estimate as explained in Complement 5.6.4.

To reduce the computational burden of the above algorithm we can run it with a value of K that is not much larger than N (*e.g.*, $K \in [2N, 4N]$). After the iterations are terminated, the final spectral estimate can be evaluated on a (much) finer frequency grid, if desired.

A cyclic minimizer reduces the criterion function at each iteration (see the discussion in Complement 4.9.5). Furthermore, in the present case this reduction is strict because the solutions to the minimization problems with respect to y_u and to $\{h(\omega_k), \beta(\omega_k)\}$ in Steps 1 and 2 are unique under weak conditions. Combining this observation with the fact that the criterion in (5.6.57) is bounded from below by zero, we can conclude that the GAPES algorithm converges to a minimum point of (5.6.57). This minimum may be a local or global minimum, depending in part on the quality of the initial estimates of $\{h(\omega_k), \beta(\omega_k)\}$ used in Step 0. The initialization step, as well as the remaining steps in the GAPES algorithm, are discussed in more detail below.

Step 0. A simple way to obtain initial estimates of $\{h(\omega_k), \beta(\omega_k)\}$ is to apply APES to the full-data sequence with $y_u = 0$. This way of initializing GAPES can be interpreted as permuting Step 1 with Step 2 in the algorithm and initializing the algorithm in Step 0 with $y_u = 0$.

A more elaborate initialization scheme consists of using only the available data samples to build the sample covariance matrix $\hat{R}$ in (5.6.47) needed in APES. Provided that there are enough samples so that the resulting $\hat{R}$ matrix is nonsingular, this initialization scheme usually gives more accurate estimates of $\{h(\omega_k), \beta(\omega_k)\}$ than the ones obtained by setting $y_u = 0$ (see [Stoica, Larsson, and Li 2000] for details).

Step 1. We want to find the solution $\hat{y}_u$ to the problem:

$$\min_{y_u} \sum_{k=1}^{K} \sum_{t=m+1}^{N} \left| \hat{h}^*(\omega_k)\tilde{y}(t) - \hat{\beta}(\omega_k) e^{i\omega_k t} \right|^2 \tag{5.6.58}$$

where $\tilde{y}(t) = [y(t), y(t-1), \ldots, y(t-m)]^T$. We will show that the above minimization problem is quadratic in y_u (for given $\{\hat{h}(\omega_k)\}$ and $\{\hat{\beta}(\omega_k)\}$), and thus admits a closed-form solution.

Let $\hat{h}^*(\omega_k) = [h_{0,k}, h_{1,k}, \ldots, h_{m,k}]$ and define

$$H_k = \begin{bmatrix} h_{0,k} & h_{1,k} & \cdots & h_{m,k} & & 0 \\ & \ddots & \ddots & & \ddots & \\ 0 & & h_{0,k} & h_{1,k} & \cdots & h_{m,k} \end{bmatrix}, \qquad (N-m) \times N$$

$$\mu_k = \hat{\beta}(\omega_k) \begin{bmatrix} e^{i\omega_k N} \\ \vdots \\ e^{i\omega_k (m+1)} \end{bmatrix}, \qquad (N-m) \times 1$$

Using this notation we can write the quadratic criterion in (5.6.58) as

$$\sum_{k=1}^{K} \left\| H_k \begin{bmatrix} y(N) \\ \vdots \\ y(1) \end{bmatrix} - \mu_k \right\|^2 \tag{5.6.59}$$

Next, we define the matrices A_k and U_k via the following equality:

$$H_k \begin{bmatrix} y(N) \\ \vdots \\ y(1) \end{bmatrix} = A_k y_a + U_k y_u \tag{5.6.60}$$

With this notation, the criterion in (5.6.59) becomes:

$$\sum_{k=1}^{K} \| U_k y_u - (\mu_k - A_k y_a) \|^2 \tag{5.6.61}$$

The minimizer of (5.6.61) with respect to y_u is readily found to be (see Result R32 in Appendix A):

$$\hat{y}_u = \left[\sum_{k=1}^{K} U_k^* U_k \right]^{-1} \left[\sum_{k=1}^{K} U_k^* (\mu_k - A_k y_a) \right] \tag{5.6.62}$$

The inverse matrix above exists under weak conditions; for details, see [Stoica, Larsson, and Li 2000].

Step 2. The solution to this step can be computed by applying the APES algorithm in Complement 5.6.4 to the data sequence made from y_a and $\hat{y}_u$.

The description of the GAPES algorithm in now complete. Numerical experience with this algorithm, reported in [Stoica, Larsson, and Li 2000], suggests that GAPES has good performance, particularly for data consisting of a mixture of sinusoidal signals superimposed in noise.

5.6.6 Extensions of Filter Bank Approaches to Two–Dimensional Signals

The following filter bank approaches for one-dimensional (1D) signals were discussed so far in this chapter and its complements:

- the periodogram,
- the refined filter bank method,
- the Capon method, and
- the APES method

In this complement we will explain briefly how the above *nonparametric* spectral analysis methods can be extended to the case of two–dimensional (2D) signals. In the process, we also provide new interpretations for some of these methods, which are particularly useful when we want very simple (although somewhat heuristic) derivations of the methods in question. We will in turn discuss the extension of each of the methods listed above. Note that 2D spectral analysis finds applications in image processing, synthetic aperture radar imagery, and so forth. See [Larsson, Li, and Stoica 2003] for a review that covers the 2D methods discussed in this complement, and their application to synthetic aperture radar. The 2D extension of some *parametric* methods for spectral line analysis is discussed in Complement 4.9.7.

Periodogram

The 1D periodogram can be obtained by a least-squares (LS) fitting of the data $\{y(t)\}$ to a generic 1D sinusoidal sequence $\{\beta e^{i\omega t}\}$:

$$\min_{\beta} \sum_{t=1}^{N} \left| y(t) - \beta e^{i\omega t} \right|^2 \tag{5.6.63}$$

The solution to (5.6.63) is readily found to be

$$\beta(\omega) = \frac{1}{N} \sum_{t=1}^{N} y(t) e^{-i\omega t} \tag{5.6.64}$$

The squared modulus of (5.6.64) (scaled by N; see Section 5.2) gives the 1D periodogram

$$\frac{1}{N} \left| \sum_{t=1}^{N} y(t) e^{-i\omega t} \right|^2 \tag{5.6.65}$$

In the 2D case, let $\{y(t, \bar{t}\,)\}$ (for $t = 1, \ldots, N$ and $\bar{t} = 1, \ldots, \bar{N}$) denote the available data matrix, and let $\{\beta e^{i(\omega t + \bar{\omega}\bar{t}\,)}\}$ denote a generic 2D sinusoid. The LS fit of the data to the generic sinusoid, that is:

$$\min_{\beta} \sum_{t=1}^{N} \sum_{\bar{t}=1}^{\bar{N}} \left| y(t, \bar{t}\,) - \beta e^{i(\omega t + \bar{\omega}\bar{t}\,)} \right|^2 \iff \min_{\beta} \sum_{t=1}^{N} \sum_{\bar{t}=1}^{\bar{N}} \left| y(t, \bar{t}\,) e^{-i(\omega t + \bar{\omega}\bar{t}\,)} - \beta \right|^2 \tag{5.6.66}$$

has the following solution:

$$\beta(\omega,\bar{\omega}) = \frac{1}{N\bar{N}} \sum_{t=1}^{N} \sum_{\bar{t}=1}^{\bar{N}} y(t,\bar{t}\,) e^{-i(\omega t + \bar{\omega}\bar{t}\,)} \tag{5.6.67}$$

Similarly to the 1D case, the scaled squared magnitude of (5.6.67) yields the *2D periodogram*

$$\boxed{\frac{1}{N\bar{N}} \left| \sum_{t=1}^{N} \sum_{\bar{t}=1}^{\bar{N}} y(t,\bar{t}\,) e^{-i(\omega t + \bar{\omega}\bar{t}\,)} \right|^2} \tag{5.6.68}$$

which can be efficiently computed by means of a 2D FFT algorithm as described below.

The 2D FFT algorithm computes the 2D DTFT of a sequence $\{y(t,\bar{t}\,)\}$ (for $t = 1,\ldots,N$; $\bar{t} = 1,\ldots,\bar{N}$) on a grid of frequency values defined by

$$\begin{aligned} \omega_k &= \frac{2\pi k}{N}, \qquad k = 0,\ldots,N-1 \\ \bar{\omega}_\ell &= \frac{2\pi \ell}{\bar{N}}, \qquad \ell = 0,\ldots,\bar{N}-1 \end{aligned}$$

The 2D FFT algorithm achieves computational efficiency by making use of the 1D FFT described in Section 2.3. Let

$$\begin{aligned} Y(k,\ell) &= \sum_{t=1}^{N} \sum_{\bar{t}=1}^{\bar{N}} y(t,\bar{t}\,) e^{-i\left(\frac{2\pi k}{N} t + \frac{2\pi \ell}{\bar{N}} \bar{t}\right)} \\ &= \sum_{t=1}^{N} e^{-i\frac{2\pi k}{N} t} \underbrace{\sum_{\bar{t}=1}^{\bar{N}} y(t,\bar{t}\,) e^{-i\frac{2\pi \ell}{\bar{N}} \bar{t}}}_{\triangleq V_t(\ell)} \qquad (5.6.69) \\ &= \sum_{t=1}^{N} V_t(\ell) e^{-i\frac{2\pi k}{N} t} \qquad (5.6.70) \end{aligned}$$

For each $t = 1,\ldots,N$, the sequence $\{V_t(\ell)\}_{\ell=0}^{\bar{N}-1}$ defined in (5.6.69) can be efficiently computed using a 1D FFT of length $\bar{N}$ (*cf.* Section 2.3). In addition, for each $\ell = 0,\ldots,\bar{N}-1$, the sum in (5.6.70) can be efficiently computed using a 1D FFT of length N. If N is a power of two, an N-point 1D FFT requires $\frac{N}{2}\log_2 N$ flops. Thus, if N and $\bar{N}$ are powers of two, then the number of operations needed to compute $\{Y(k,\ell)\}$ is

$$\boxed{N\frac{\bar{N}}{2}\log_2 \bar{N} + \bar{N}\frac{N}{2}\log_2 N = \frac{N\bar{N}}{2}\log_2(N\bar{N}) \text{ flops}} \tag{5.6.71}$$

If N or $\bar{N}$ is not a power of two, zero padding can be used.

Refined Filter Bank (RFB) Method

Similarly to the 1D case (see (5.3.30) or (5.7.1)), the *2D RFB method* can be implemented as a multiwindowed periodogram (*cf.* (5.6.68)):

$$\boxed{\frac{1}{K}\sum_{p=1}^{K}\left|\sum_{t=1}^{N}\sum_{\bar{t}=1}^{\bar{N}} w_p(t,\bar{t}\,)\,y(t,\bar{t}\,)\,e^{-i(\omega t+\bar{\omega}\bar{t}\,)}\right|^2} \tag{5.6.72}$$

where $\{w_p(t,\bar{t}\,)\}_{p=1}^{K}$ are the 2D Slepian data windows (or tapers). The problem left is to derive 2D extensions of the 1D Slepian tapers discussed in Section 5.3.1.

The frequency response of a 2D taper $\{w(t,\bar{t}\,)\}$ is given by

$$\sum_{t=1}^{N}\sum_{\bar{t}=1}^{\bar{N}} w(t,\bar{t}\,)e^{-i(\omega t+\bar{\omega}\bar{t}\,)} \tag{5.6.73}$$

Let us define the matrices

$$W=\begin{bmatrix} w(1,1) & \cdots & w(1,\bar{N}) \\ \vdots & & \vdots \\ w(N,1) & \cdots & w(N,\bar{N}) \end{bmatrix}$$

$$B=\begin{bmatrix} e^{-i(\omega+\bar{\omega})} & \dots & e^{-i(\omega+\bar{\omega}\bar{N})} \\ \vdots & & \vdots \\ e^{-i(\omega N+\bar{\omega})} & \dots & e^{-i(\omega N+\bar{\omega}\bar{N})} \end{bmatrix}$$

and let vec$(\cdot)$ denote the vectorizaton operator which stacks the columns of its matrix argument into a single vector. Also, let

$$a(\omega)=\begin{bmatrix} e^{-i\omega} \\ \vdots \\ e^{-iN\omega} \end{bmatrix}, \qquad \bar{a}(\bar{\omega})=\begin{bmatrix} e^{-i\bar{\omega}} \\ \vdots \\ e^{-i\bar{N}\bar{\omega}} \end{bmatrix} \tag{5.6.74}$$

and let the symbol $\otimes$ denote the Kronecker matrix product; the Kronecker product of two matrices, X of size $m\times n$ and Y of size $\bar{m}\times\bar{n}$, is an $m\bar{m}\times n\bar{n}$ matrix whose (i,j) block of size $\bar{m}\times\bar{n}$ is given by $X_{ij}\cdot Y$, for $i=1,\dots,m$ and $j=1,\dots,n$, where X_{ij} denotes the (i,j)th element of X (see, *e.g.*, [Horn and Johnson 1985] for the properties of $\otimes$). Finally, let

$$\begin{aligned} w &= \text{vec}(W) \\ &= \big[w(1,1),\dots,w(N,1)|\cdots|w(1,\bar{N}),\dots,w(N,\bar{N})\big]^T \end{aligned} \tag{5.6.75}$$

and

$$\begin{aligned} b(\omega,\bar{\omega}) &= \text{vec}(B) \\ &= \Big[e^{-i(\omega+\bar{\omega})},\dots,e^{-i(\omega N+\bar{\omega})}|\cdots|e^{-i(\omega+\bar{\omega}\bar{N})},\dots,e^{-i(\omega N+\bar{\omega}\bar{N})}\Big]^T \\ &= \bar{a}(\bar{\omega})\otimes a(\omega) \end{aligned} \tag{5.6.76}$$

(the last equality in (5.6.76) follows from the definition of $\otimes$). Using (5.6.75) and (5.6.76), we can write (5.6.73) as

$$w^* b(\omega, \bar{\omega}) \tag{5.6.77}$$

which is similar to the expression $h^* a(\omega)$ for the 1D frequency response in Section 5.3.1. Hence, the analysis in Section 5.3.1 carries over to the 2D case, with the only difference that now the matrix Γ is given by

$$\begin{aligned}\Gamma_{2D} &= \frac{1}{(2\pi)^2} \int_{-\beta\pi}^{\beta\pi} \int_{-\bar{\beta}\pi}^{\bar{\beta}\pi} b(\omega, \bar{\omega}) b^*(\omega, \bar{\omega}) d\omega \, d\bar{\omega} \\ &= \frac{1}{(2\pi)^2} \int_{-\beta\pi}^{\beta\pi} \int_{-\bar{\beta}\pi}^{\bar{\beta}\pi} [\bar{a}(\bar{\omega}) \bar{a}^*(\bar{\omega})] \otimes [a(\omega) a^*(\omega)] \, d\omega \, d\bar{\omega}\end{aligned}$$

where we have used the fact that $(A \otimes B)(C \otimes D) = AC \otimes BD$ for any conformable matrices (see, *e.g.*, [Horn and Johnson 1985]). Hence,

$$\boxed{\Gamma_{2D} = \bar{\Gamma}_{1D} \otimes \Gamma_{1D}} \tag{5.6.78}$$

where

$$\Gamma_{1D} = \frac{1}{2\pi} \int_{-\beta\pi}^{\beta\pi} a(\omega) a^*(\omega) d\omega, \qquad \bar{\Gamma}_{1D} = \frac{1}{2\pi} \int_{-\bar{\beta}\pi}^{\bar{\beta}\pi} \bar{a}(\bar{\omega}) \bar{a}^*(\bar{\omega}) d\bar{\omega} \tag{5.6.79}$$

The above Kronecker product expression of Γ_{2D} implies that (see [Horn and Johnson 1985]):

(a) The eigenvalues of Γ_{2D} are equal to the products of the eigenvalues of Γ_{1D} and $\bar{\Gamma}_{1D}$.

(b) The eigenvectors of Γ_{2D} are given by the Kronecker products of the eigenvectors of Γ_{1D} and $\bar{\Gamma}_{1D}$.

The conclusion is that *the computation of 2D Slepian tapers can be reduced to the computation of 1D Slepian tapers*. We refer the reader to Section 5.3.1, and the references cited there, for details on 1D Slepian taper computation.

Capon and APES Methods

In the 1D case we can obtain the Capon and APES methods by a weighted LS fit of the data vectors $\{\tilde{y}(t)\}$, where

$$\tilde{y}(t) = [y(t), y(t-1), \ldots, y(t-m)]^T \tag{5.6.80}$$

to the vectors corresponding to a generic sinusoidal signal with frequency ω. Specifically, consider the LS problem:

$$\min_{\beta} \sum_{t=m+1}^{N} \left[\tilde{y}(t) - a(\omega)\beta e^{i\omega t}\right]^* W^{-1} \left[\tilde{y}(t) - a(\omega)\beta e^{i\omega t}\right] \tag{5.6.81}$$

where W^{-1} is a weighting matrix which is yet to be specified, and where

$$a(\omega) = \left[1, e^{-i\omega}, \ldots, e^{-im\omega}\right]^T \tag{5.6.82}$$

Note that the definition of $a(\omega)$ in (5.6.82) differs from that of $a(\omega)$ in (5.6.74). The solution to (5.6.81) is given by

$$\beta(\omega) = \frac{a^*(\omega)W^{-1}g(\omega)}{a^*(\omega)W^{-1}a(\omega)} \tag{5.6.83}$$

where

$$g(\omega) = \frac{1}{N-m}\sum_{t=m+1}^{N} \tilde{y}(t)e^{-i\omega t} \tag{5.6.84}$$

For

$$W = \hat{R} \triangleq \frac{1}{N-m}\sum_{t=m+1}^{N} \tilde{y}(t)\tilde{y}^*(t) \tag{5.6.85}$$

the weighted LS estimate of the amplitude spectrum in (5.6.83) reduces to the Capon method (see equation (5.6.55) in Complement 5.6.4), whereas for

$$W = \hat{R} - g(\omega)g^*(\omega) \triangleq \hat{Q}(\omega) \tag{5.6.86}$$

equation (5.6.83) gives the APES method (see equations (5.6.48), (5.6.49), and (5.6.51) in Complement 5.6.4).

The extension of the above derivation to the 2D case is straightforward. By analogy with the 1D data vector in (5.6.80), let

$$\left[y(t-k, \bar{t}-\bar{k})\right] = \begin{bmatrix} y(t,\bar{t}) & \cdots & y(t,\bar{t}-\bar{m}) \\ \vdots & & \vdots \\ y(t-m,\bar{t}) & \cdots & y(t-m,\bar{t}-\bar{m}) \end{bmatrix} \tag{5.6.87}$$

be the 2D data matrix, and let

$$\begin{aligned} \tilde{y}(t,\bar{t}) &= \operatorname{vec}\left(\left[y(t-k,\bar{t}-\bar{k})\right]\right) \\ &= \left[y(t,\bar{t}), \ldots, y(t-m,\bar{t})|\cdots|y(t,\bar{t}-\bar{m}), \ldots, y(t-m,\bar{t}-\bar{m})\right]^T \end{aligned} \tag{5.6.88}$$

Our goal is to fit the data matrix in (5.6.87) to the matrix corresponding to a generic 2D sinusoid with frequency pair $(\omega, \bar{\omega})$, that is:

$$\left[\beta e^{i[\omega(t-k)+\bar{\omega}(\bar{t}-\bar{k})]}\right] = \beta \begin{bmatrix} e^{i[\omega t+\bar{\omega}\bar{t}]} & \cdots & e^{i[\omega t+\bar{\omega}(\bar{t}-\bar{m})]} \\ \vdots & & \vdots \\ e^{i[\omega(t-m)+\bar{\omega}\bar{t}]} & \cdots & e^{i[\omega(t-m)+\bar{\omega}(\bar{t}-\bar{m})]} \end{bmatrix} \tag{5.6.89}$$

Similarly to (5.6.88), let us vectorize (5.6.89):

$$\begin{aligned} \operatorname{vec}\left(\left[\beta e^{i[\omega(t-k)+\bar{\omega}(\bar{t}-\bar{k})]}\right]\right) &= \beta e^{i(\omega t+\bar{\omega}\bar{t})}\operatorname{vec}\left(\left[e^{-i(\omega k+\bar{\omega}\bar{k})}\right]\right) \\ &= \beta e^{i(\omega t+\bar{\omega}\bar{t})}\bar{a}(\bar{\omega}) \otimes a(\omega) \end{aligned} \tag{5.6.90}$$

As in (5.6.76), let

$$\boxed{b(\omega,\bar{\omega}) = \bar{a}(\bar{\omega}) \otimes a(\omega), \qquad (m+1)(\bar{m}+1) \times 1} \tag{5.6.91}$$

We deduce from (5.6.88)–(5.6.91) that the 2D counterpart of the 1D weighted LS fitting problem in (5.6.81) is the following:

$$\begin{aligned} \min_{\beta} \sum_{t=m+1}^{N} \sum_{\bar{t}=\bar{m}+1}^{\bar{N}} & \left[\tilde{y}(t,\bar{t}\,) - \beta e^{i(\omega t+\bar{\omega}\bar{t}\,)} b(\omega,\bar{\omega})\right]^{*} W^{-1} \\ & \cdot \left[\tilde{y}(t,\bar{t}\,) - \beta e^{i(\omega t+\bar{\omega}\bar{t}\,)} b(\omega,\bar{\omega})\right] \end{aligned} \tag{5.6.92}$$

The solution to (5.6.92) is given by:

$$\boxed{\beta(\omega,\bar{\omega}) = \frac{b^{*}(\omega,\bar{\omega}) W^{-1} g(\omega,\bar{\omega})}{b^{*}(\omega,\bar{\omega}) W^{-1} b(\omega,\bar{\omega})}} \tag{5.6.93}$$

where

$$\boxed{g(\omega,\bar{\omega}) = \frac{1}{(N-m)(\bar{N}-\bar{m}\,)} \sum_{t=m+1}^{N} \sum_{\bar{t}=\bar{m}+1}^{\bar{N}} \tilde{y}(t,\bar{t}\,) e^{-i(\omega t+\bar{\omega}\bar{t}\,)}} \tag{5.6.94}$$

The *2D Capon method* is given by (5.6.93) with

$$\boxed{W = \frac{1}{(N-m)(\bar{N}-\bar{m}\,)} \sum_{t=m+1}^{N} \sum_{\bar{t}=\bar{m}+1}^{\bar{N}} \tilde{y}(t,\bar{t}\,) \tilde{y}^{*}(t,\bar{t}\,) \triangleq \hat{R}} \tag{5.6.95}$$

whereas the *2D APES method* is given by (5.6.93) with

$$\boxed{W = \hat{R} - g(\omega,\bar{\omega}) g^{*}(\omega,\bar{\omega}) \triangleq \hat{Q}(\omega,\bar{\omega})} \tag{5.6.96}$$

Note that $g(\omega,\bar{\omega})$ in (5.6.94) can be efficiently evaluated using a 2D FFT algorithm. However, an efficient implementation of the 2D spectral estimate in (5.6.93) is not so direct. A naive implementation may be rather time consuming owing to the large dimensions of the vectors and matrices involved, as well as the need to evaluate $\beta(\omega,\bar{\omega})$ on a 2D frequency grid. We refer the reader to [Larsson, Li, and Stoica 2003] and the references therein for a discussion of computationally efficient implementations of 2D Capon and 2D APES spectral estimation methods.

5.7 EXERCISES

Exercise 5.1: Multiwindow Interpretation of Bartlett and Welch Methods

Equation (5.3.30) allows us to interpret the RFB method as a *multiwindow* (or *multitaper*) approach. Indeed, according to equation (5.3.30), we can write the RFB spectral estimator as:

$$\hat{\phi}(\omega) = \frac{1}{K} \sum_{p=1}^{K} \left| \sum_{t=1}^{N} w_{p,t} y(t) e^{-i\omega t} \right|^2 \tag{5.7.1}$$

where K is the number of data windows (or tapers), and where in the case of RFB the $w_{p,t}$ are obtained from the pth dominant Slepian sequence ($p = 1, \ldots, K$).

Show that the Bartlett and Welch methods can also be cast into the previous multiwindow framework. Make use of the multiwindow interpretation of these methods to compare them with one another and with the RFB approach.

Exercise 5.2: An Alternative Statistically Stable RFB Estimate

In Section 5.3.3 we developed a statistically stable RFB spectral estimator using a bank of narrow bandpass filters. In Section 5.4 we derived the Capon method, which employs a shorter filter length than the RFB. In this exercise we derive the RFB analog of the Capon approach and show its correspondence with the Welch and Blackman–Tukey estimators.

As an alternative technique to the filter in (5.3.4), consider a passband filter of shorter length:

$$h = [h_0, \ldots, h_m]^* \tag{5.7.2}$$

for some $m < N$. The optimal h will be the first Slepian sequence in (5.3.10) found using a Γ matrix of size $m \times m$. In this case, the filtered output

$$y_F(t) = \sum_{k=0}^{m} h_k \tilde{y}(t-k) \tag{5.7.3}$$

(with $\tilde{y}(t) = y(t)e^{-i\omega t}$) can be computed for $t = m+1, \ldots, N$. The resulting RFB spectral estimate is given by

$$\hat{\phi}(\omega) = \frac{1}{N-m} \sum_{t=m+1}^{N} |y_F(t)|^2 \tag{5.7.4}$$

(a) Show that the estimator in (5.7.4) is an unbiased estimate of $\phi(\omega)$, under the standard assumptions considered in this chapter.

(b) Show that $\hat{\phi}(\omega)$ can be written as

$$\hat{\phi}(\omega) = \frac{1}{m+1} h^*(\omega) \hat{R}\, h(\omega) \tag{5.7.5}$$

where $\hat{R}$ is an $(m+1) \times (m+1)$ Hermitian (but not Toeplitz) estimate of the covariance matrix of $y(t)$. Find the corresponding filter $h(\omega)$.

(c) Compare (5.7.5) with the Blackman–Tukey estimate in equation (5.4.22). Discuss how the two compare when N is large.

(d) Interpret $\hat{\phi}(\omega)$ as a Welch–type estimator. What is the overlap parameter K in the corresponding Welch method?

Exercise 5.3: Another Derivation of the Capon FIR Filter

The Capon FIR filter design problem can be restated as follows:

$$\min_h \; h^* R h / |h^* a(\omega)|^2 \tag{5.7.6}$$

Make use of the Cauchy–Schwartz inequality (Result R22 in Appendix A) to obtain a simple proof of the fact that h given by (5.4.8) is a solution to the optimization problem above.

Exercise 5.4: The Capon Filter is a Matched Filter

Compare the Capon filter design problem (5.4.7) with the following classical *matched filter design*.

- Filter: A causal FIR filter with an $(m+1)$–dimensional impulse response vector denoted by h.
- Signal–in–noise model: $y(t) = \alpha e^{i\omega t} + \varepsilon(t)$, which gives the following expression for the input vector to the filter:

$$z(t) = \alpha a(\omega) e^{i\omega t} + e(t) \tag{5.7.7}$$

  where $a(\omega)$ is as defined in (5.4.6), $\alpha e^{i\omega t}$ is a sinusoidal signal,

$$z(t) = [y(t), y(t-1), \ldots, y(t-m)]^T$$

  and $e(t)$ is a possibly colored noise vector defined similarly to $z(t)$. The signal and noise terms above are assumed to be uncorrelated.

- Design goal: Maximize the signal–to–noise ratio in the filter's output,

$$\max_h |h^* a(\omega)|^2 / h^* Q h \tag{5.7.8}$$

  where Q is the noise covariance matrix.

Show that the Capon filter is identical to the matched filter which solves the above design problem. The adjective "matched" attached to the above filter is motivated by the fact that the filter impulse response vector h depends on, and hence is "matched to", the signal term in (5.7.7).

Exercise 5.5: Computation of the Capon Spectrum

The Capon spectral estimators are defined in equations (5.4.19) and (5.4.20). The bulk of the computation of either estimator consists in the evaluation of an expression of the form $a^*(\omega) Q a(\omega)$, where Q is a given positive definite matrix, at

a number of points on the frequency axis. Let these evaluation points be given by $\{\omega_k = 2\pi k/M\}_{k=0}^{M-1}$ for some sufficiently large M value (which we assume to be a power of two). The direct evaluation of $a^*(\omega_k)Qa(\omega_k)$, for $k = 0, \ldots, M-1$, would require $\mathcal{O}(Mm^2)$ flops. Show that an evaluation based on the eigendecomposition of Q and the use of FFT is usually much more efficient computationally.

Exercise 5.6: A Relationship between the Capon Method and MUSIC (Pseudo)Spectra

Assume that the covariance matrix R, entering the Capon spectrum formula, has the expression (4.2.7) in the frequency estimation application. Then, show that

$$\lim_{\sigma^2 \to 0} (\sigma^2 R^{-1}) = I - A(A^*A)^{-1}A^* \tag{5.7.9}$$

Conclude that the limiting (for $N \gg 1$) Capon and MUSIC (pseudo)spectra, associated with the frequency estimation data, are close to one another, provided that all signal–to–noise ratios are large enough.

Exercise 5.7: A Capon–like Implementation of MUSIC

The Capon and MUSIC (pseudo)spectra, as the data length N increases, are given by the functions in equations (5.4.12) and (4.5.13), respectively. Recall that the columns of the matrix G in (4.5.13) are equal to the $(m-n)$ eigenvectors corresponding to the smallest eigenvalues of the covariance matrix R in (5.4.12).

Consider the following Capon–like pseudospectrum:

$$g_k(\omega) = a^*(\omega)R^{-k}a(\omega)\lambda^k \tag{5.7.10}$$

where λ is the minimum eigenvalue of R; the covariance matrix R is assumed to have the form (4.2.7) postulated by MUSIC. Show that, under this assumption,

$$\boxed{\lim_{k \to \infty} g_k(\omega) = a^*(\omega)GG^*a(\omega) = (4.5.13)} \tag{5.7.11}$$

(where the convergence is uniform in ω). Explain why the convergence in (5.7.11) may be slow in difficult scenarios, such as those with closely spaced frequencies, and hence the use of (5.7.10) with a large k to approximate the MUSIC pseudospectrum may be computationally inefficient. However, the use of (5.7.10) for frequency estimation has a potential advantage over MUSIC that may outweigh its computational inefficiency. Find and comment on that advantage.

Exercise 5.8: Capon Estimate of the Parameters of a Single Sine Wave

Assume that the data under study consists of a sinusoidal signal observed in white noise. In such a case, the covariance matrix R is given by (*cf.* (4.2.7)):

$$R = \alpha^2 a(\omega_0)a(\omega_0)^* + \sigma^2 I, \qquad (m \times m)$$

where ω_0 denotes the true frequency value. Show that the limiting (as $N \to \infty$) Capon spectrum (5.4.12) peaks at $\omega = \omega_0$. Derive the height of the peak and show

that it is not equal to α^2 (as might have been expected) but is given by a function of α^2, m and σ^2. Conclude that the Capon method can be used to obtain a consistent estimate of the frequency of a *single* sinusoidal signal in white noise (but not of the signal power).

We note that, for two or more sinusoidal signals, the Capon frequency estimates are inconsistent. Hence the Capon frequency estimator behaves somewhat similarly to the AR frequency estimation method in this respect; see Exercise 4.4.

Exercise 5.9: An Alternative Derivation of the Relationship between the Capon and AR Methods

Make use of the equation (3.9.17) relating R_{m+1}^{-1} to R_m^{-1} to obtain a simple proof of the formula (5.4.36) relating the Capon and AR spectral estimators.

COMPUTER EXERCISES

Tools for Filter Bank Spectral Estimation:

The text web site `www.prenhall.com/stoica` contains the following MATLAB functions for use in computing filter bank spectral estimates.

- `h=slepian(N,K,J)`
  Returns the first `J` Slepian sequences given `N` and `K` as defined in Section 5.3; `h` is an $N \times J$ matrix whose ith column gives the ith Slepian sequence.

- `phi=rfb(y,K,L)`
  The RFB spectral estimator. The vector `y` is the input data vector, `L` controls the frequency sample spacing of the output, and the output vector `phi`$= \hat{\phi}(\omega_k)$ where $\omega_k = \frac{2\pi k}{L}$. For $K = 1$, this function implements the high resolution RFB method in equation (5.3.22), and for $K > 1$ it implements the statistically stable RFB method.

- `phi=capon(y,m,L)`
  The CM Version–1 spectral estimator in equation (5.4.19); `y`, `L`, and `phi` are as for the RFB spectral estimator, and `m` is the size of the square matrix $\hat{R}$.

Exercise C5.10: Slepian Window Sequences

We consider the Slepian window sequences for both $K = 1$ (high resolution) and $K = 4$ (lower resolution, higher statistical stability) and compare them with classical window sequences.

(a) Evaluate and plot the first 8 Slepian window sequences and their Fourier transforms for $K = 1$ and 4 and for $N = 32$, 64, and 128 (and perhaps other values, too). Qualitatively describe the filter passbands of these first 8 Slepian sequences for $K = 1$ and $K = 4$. Which act as lowpass filters and which act as "other" types of filters?

(b) In this chapter we showed that for "large N" and $K = 1$, the first Slepian sequence is "reasonably close to" the rectangular window; compare the first

Slepian sequence and its Fourier transform for $N = 32$, 64, and 128 to the rectangular window and its Fourier transform. How do they compare as a function of N? Based on this comparison, how do you expect the high resolution RFB PSD estimator to perform relative to the periodogram?

Exercise C5.11: Resolution of Refined Filter Bank Methods

We will compare the resolving power of the RFB spectral estimator with $K = 1$ to that of the periodogram. To do so we look at the spectral estimates of sequences which are made up of two sinusoids in noise, and where we vary the frequency difference.

Generate the sequences

$$y_\alpha(t) = 10\sin(0.2 \cdot 2\pi t) + 5\sin((0.2 + \alpha/N)2\pi t)$$

for various values of α near 1. Compare the resolving ability of the RFB power spectral estimate for $K = 1$ and of the periodogram for both $N = 32$ and $N = 128$. Discuss your results in relation to the theoretical comparisons between the two estimators. Do the results echo the theoretical predictions based on the analysis of Slepian sequences?

Exercise C5.12: The Statistically Stable RFB Power Spectral Estimator

In this exercise we will compare the RFB power spectral estimator when $K = 4$ to the Blackman–Tukey and Daniell estimators. We will use the narrowband and broadband processes considered in Exercise C2.22.

Broadband ARMA Process:

(a) Generate 50 realizations of the broadband ARMA process in Exercise C2.22, using $N = 256$. Estimate the spectrum using:

- The RFB method with $K = 4$.
- The Blackman–Tukey method with an appropriate window (such as the Bartlett window) and window length M. Choose M to obtain similar performance to the RFB method (you can select an appropriate value of M off–line and verify it in your experiments).
- The Daniell method with $\tilde{N} = 8N$ and an appropriate choice of J. Choose J to obtain similar performance to the RFB method (you can select J off–line and verify it in your experiments).

(b) Evaluate the relative performance of the three estimators in terms of bias and variance. Are the comparisons in agreement with the theoretical predictions?

Narrowband ARMA Process: Repeat parts (a) and (b) above using 50 realizations (with $N = 256$) of the narrowband ARMA process in Exercise C2.22.

Exercise C5.13: The Capon Method

In this exercise we compare the Capon method to the RFB and AR methods. Consider the sinusoidal data sequence in equation (2.9.20) from Exercise C2.19, with $N = 64$.

(a) We first compare the data filters corresponding to a RFB method (in which the filter is data independent) with the filter corresponding to the CM Version–1 method using both $m = N/4$ and $m = N/2 - 1$; we choose the Slepian RFB method with $K = 1$ and $K = 4$ for this comparison. For two estimation frequencies, $\omega = 0$ and $\omega = 2\pi \cdot 0.1$, plot the frequency response of the five filters (1 for $K = 1$ and 4 for $K = 4$) shown in the first block of Figure 5.1 for the two RFB methods, and also plot the response of the two Capon filters (one for each value of m; see (5.4.5) and (5.4.8)). What are their characteristic features in relation to the data? Based on these plots, discuss how data dependence can improve spectral estimation performance.

(b) Compare the two Capon estimators with the RFB estimator for both $K = 1$ and $K = 4$. Generate 50 Monte–Carlo realizations of the data and overlay plots of the 50 spectral estimates for each estimator. Discuss the similarities and differences between the RFB and Capon estimators.

(c) Compare Capon and Least Squares AR spectral estimates, again by generating 50 Monte–Carlo realizations of the data and overlaying plots of the 50 spectral estimates. Use $m = 8$, 16, and 30 for both the Capon method and the AR model order. How do the two methods compare in terms of resolution and variance? What are your main summarizing conclusions? Explain your results in terms of the data characteristics.